AD-A160 424 THE ROLE OF EIGENSOLUTIONS IN NONLINEAR INVERSE CAVITY-FLOW-THEORY REVISI..(U) PENNSYLVANIA STATE UNIV UNIVERSITY PARK APPLIED RESEARCH LAB.. B R PARKIN 1/1

UNCLASSIFIED 10 JUN 85 ARL/PSU/TM-85-97 N00024-79-C-6043 F/G 20/4 NL

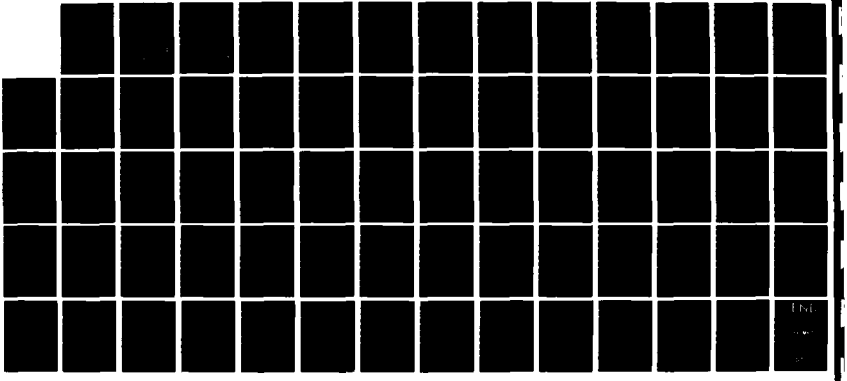

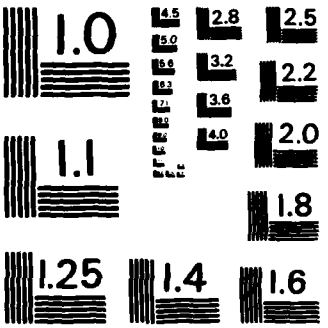

MICROCOPY RESOLUTION TEST CHART
NATIONAL BUREAU OF STANDARDS - 1963 - A

REPRODUCED AT GOVERNMENT EXPENSE

AD-A160 424

THE ROLE OF EIGENSOLUTIONS IN NONLINEAR INVERSE CAVITY-FLOW THEORY [REVISED]

B. R. Parkin

Technical Memorandum
File No. TM 85-97
10 June 1985
Contract N00024-79-C-6043

Copy No. 5

The Pennsylvania State University
Intercollege Research Programs and Facilities
APPLIED RESEARCH LABORATORY
Post Office Box 30
State College, Pa. 16804

DTIC ELECTE OCT 17 1985 S B D

DTIC FILE COPY

DISTRIBUTION STATEMENT A
Approved for public release;
Distribution Unlimited

85 10 16 140

THE ROLE OF EIGENSOLUTIONS IN NONLINEAR INVERSE CAVITY-FLOW THEORY [REVISED]

B. R. Parkin

Technical Memorandum
File No. TM 85-97
10 June 1985
Contract N00024-79-C-6043

Copy No. 5

Approved for public release
Distribution unlimited

The Pennsylvania State University
Intercollege Research Programs and Facilities
APPLIED RESEARCH LABORATORY
Post Office Box 30
State College, PA 16804

NAVY DEPARTMENT

NAVAL SEA SYSTEMS COMMAND

DTIC
ELECTE
OCT 17 1985
S D
B

UNCLASSIFIED

SECURITY CLASSIFICATION OF THIS PAGE (When Data Entered)

REPORT DOCUMENTATION PAGE		READ INSTRUCTIONS BEFORE COMPLETING FORM
1. REPORT NUMBER TM 85-97	2. GOVT ACCESSION NO. AD-A160424	3. RECIPIENT'S CATALOG NUMBER
4. TITLE (and Subtitle) THE ROLE OF EIGENSOLUTIONS IN NONLINEAR INVERSE CAVITY-FLOW THEORY [REVISED]		5. TYPE OF REPORT & PERIOD COVERED Technical Memorandum 6. PERFORMING ORG. REPORT NUMBER
7. AUTHOR(s) Blaine R. Parkin		8. CONTRACT OR GRANT NUMBER(s) N00024-79-C-6043
9. PERFORMING ORGANIZATION NAME AND ADDRESS Applied Research Laboratory, P. O. Box 30 The Pennsylvania State University State College, PA 16804		10. PROGRAM ELEMENT, PROJECT, TASK AREA & WORK UNIT NUMBERS
11. CONTROLLING OFFICE NAME AND ADDRESS Naval Sea Systems Command, Code NSEA 63R-31 Department of the Navy Washington, DC 20362		12. REPORT DATE 10 June 1985 13. NUMBER OF PAGES 66
14. MONITORING AGENCY NAME & ADDRESS (if different from Controlling Office) David W. Taylor Naval Ship Research and Development Center, Code 1542 Department of the Navy Bethesda, MD 20084		15. SECURITY CLASS. (of this report) UNCLASSIFIED 15a. DECLASSIFICATION DOWNGRADING SCHEDULE

16. DISTRIBUTION STATEMENT (of this Report)

Approved for public release.
Distribution unlimited.
Per NAVSEA - 5 September 1985

17. DISTRIBUTION STATEMENT (of the abstract entered in Block 20, if different from Report)

18. SUPPLEMENTARY NOTES

19. KEY WORDS (Continue on reverse side if necessary and identify by block number)

cavity flows
inverse hydrofoil design
mathematical properties

20. ABSTRACT (Continue on reverse side if necessary and identify by block number)

The method of Levi Civita is applied to an isolated fully cavitating body at zero cavitation number and adapted to the solution of the inverse problem in which one prescribes the pressure distribution on the wetted surface and then calculates the shape. The novel feature of this work is the finding that the exact theory admits the existence of a "point drag" function or eigensolution. While this fact is of no particular importance in the

DD FORM 1 JAN 73 1473 EDITION OF 1 NOV 65 IS OBSOLETE

UNCLASSIFIED

SECURITY CLASSIFICATION OF THIS PAGE (When Data Entered)

classical direct problem, we already know from the linearized theory that the eigensolution plays an important role.

In the present discussion, the basic properties of the exact 'point-drag' solution are explored under the simplest of conditions. In this way, complications which arise from non-zero cavitation numbers, free surface effects, or cascade interactions are avoided. The effects of this simple eigensolution on hydrodynamic forces and cavity shape are discussed. Finally, we give a tentative example of how this eigensolution might be used in the design process. Keywords:

QUALITY INSPECTED 3

Accession For
NTIS
DTIC
Unannounced
Justification
By
Distribution/
Availability Codes
Dist
A-1

From: B. R. Parkin

Subject: The Role of Eigensolutions in Nonlinear Inverse Cavity-Flow Theory [Revised]

Abstract: The method of Levi Civita is applied to an isolated fully cavitating body at zero cavitation number and adapted to the solution of the inverse problem in which one prescribes the pressure distribution on the wetted surface and then calculates the shape. The novel feature of this work is the finding that the exact theory admits the existence of a "point drag" function or eigensolution. While this fact is of no particular importance in the classical direct problem, we already know from the linearized theory that the eigensolution plays an important role.

In the present discussion, the basic properties of the exact "point-drag" solution are explored under the simplest of conditions. In this way, complications which arise from non-zero cavitation numbers, free surface effects, or cascade interactions are avoided. The effects of this simple eigensolution on hydrodynamic forces and cavity shape are discussed. Finally, we give a tentative example of how this eigensolution might be used in the design process.

Acknowledgments: This work has been supported by the Naval Sea Systems Command, Dr. Thomas E. Peirce [NSEA 63R-31] and by the David W. Taylor Naval Ship Research & Development Center [DTNSRDC] under the General Hydrodynamics Research Program. The author is particularly pleased to acknowledge the helpful discussions of this work by Dr. Y. T. Shen of DTNSRDC and Dr. O. Furuya of Tetratech.

Principal Nomenclature

A_1	cavity detachment point near or at profile nose
A_2	cavity detachment point at profile trailing edge
$a = (\sqrt{\phi_1} - \sqrt{\phi_2})/2$	see related nomenclature below
$b = (\sqrt{\phi_2} + \sqrt{\phi_2})/2$	see related nomenclature below
C	location of eigensolution singularity on unit circle
C_D	drag coefficient
C_L	lift coefficient
$C_p(\beta)$	pressure coefficient on wetted surface
c	profile chord length, c = 1
ds	element of arc length in z-plane
E	strength of eigensolution
$F = \phi + i\psi$	complex potential in complex F-plane
ϕ	velocity potential
ψ	stream function
O	stagnation point location
O'	point at infinity in z-plane
U	free-stream velocity
W	intermediate mapping complex plane
$w = u - iv = \frac{dF}{dz}$	complex velocity
Z	intermediate mapping complex plane
$z = x + iy$	complex variable in the physical (x,y) plane

α	angle of attack
δ	angular location of stagnation point measured from negative real axis
ζ	complex variable in unit circle plane
η	normal distance from profile chord
ξ	complex semi-circle plane, $\xi = e^{i\beta}$
σ	distance along profile chord
τ	cavity thickness at trailing edge
γ	stagnation point angular location on unit circle in ζ plane ($\cos \gamma = a/b$)
γ_c	angular location of eigensolution singularity on unit circle
ϕ_1	value of ϕ at A_1
ϕ_2	value of ϕ at A_2
$\omega(\zeta) = \theta + i\ell n\, q/U = \theta + i\tau$	complex logarithmic hodograph
θ	flow inclination
q	flow speed

Subscripts

c	pertains to eigensolution ω_c or to the cavity surface
o	pertains to flat plate solution ω_o and other variables specifically associated with the geometric point 0
0	used on any variable having zero as its argument or limit
1	pertains to regular part of solution ω_1

Introduction

The present paper bears upon the two-dimensional inverse or design problem for fully-cavitating hydrofoils in which one specifies the pressure distribution on the profile wetted surface and then calculates that wetted surface shape which will satisfy this prescription. This design problem is certainly not new to airfoil designers and as far as cavity flows are concerned, both linear and nonlinear design methods have been worked out. In the realm of nonlinear approaches to the present problem, the very general method of Yim and Higgins [1]* is worthy of note because it applies to single foils as well as to cascades of profiles for all cavitation numbers in the cavity-flow regime. Another approach has been discussed superficially by Khrabov [2]. Both of these contain far more generality than is required for this study at zero cavitation number. For the direct or off-design problem of exact cavity-flow theory, a good example of the present level of development is represented by the work of Furuya [3] and it is clear that now one can do both the design and off-design problems for fully-cavitating hydrofoils. Thus, one can attempt to tailor the profile to an entire set of performance goals and failing that he can at least design for the best compromise among a set of conflicting requirements.

According to many authors [4-7], the inverse problem is not thought to present much of a challenge at zero cavitation number. In this case, the classical method of Levi Civita [7] can be applied to an isolated body. This view is certainly proper as long as one is content, after

---

*Numbers in square brackets indicate citations in the references listed below.

prescribing the pressure in the circle plane, to accept whatever correlation between points in the circle and physical planes may result. Of course, such a rudimentary approach does not lead to a useful design procedure.

The motivation for the present investigation is that none of the literature on the nonlinearized direct and inverse problems we have surveyed so far [1-8] has made use of the fact the exact theory admits the existence of a "point drag" or complementary function. While this fact is of no particular importance in the direct problem, we have already seen in the case of the linearized inverse problem [9-11] that the complementary function can play an important role. For the exact inverse theory there has been a question if a nonlinear eigensolution exists or if it does, should it be an admissible component of the solution [1]? Therefore, in this study, we explore these questions regarding the existence and usefulness of a "point drag" or eigensolution in the nonlinear theory under the simplest set of circumstances and this leads us naturally to the restrictions that the free streamline flow pertains to an isolated profile and that the flow be at zero cavitation number. These simplifications will free us from the complications arising from non-zero cavitation numbers and other boundaries in the flow domain such as a free surface or neighboring cascade blades.

In this paper we use the term eigensolution in the sense of thin airfoil theory as suggested by the work of Van Dyke* because we already know that the inverse problem in the theory of fully cavitating hydrofoils is not necessarily unique. Our aim is to find a sufficiently weak

*Perturbation Methods in Fluid Mechanics, The Parabolic Press, Stanford, CA, pp. 48-54 (1975).

singularity which can be added to the classical Levi Civita solution and can then be used to satisfy certain additional physical conditions relating to the location of the free streamline springing from the hydrofoil nose and thereby provide a unique inverse cavity-flow solution. After we have constructed the simple eigensolution, we will examine some of its properties. The actual use of this solution in the design process will be presented elsewhere, although we will start the process so that the potential usefulness of the eigensolution in design can be seen.

Flow Geometry and Conformal Mappings

As noted above, this study uses Levi Civita's method [7] for the analysis of the exact inverse problem for a fully cavitating hydrofoil section. The flow geometry and the principal quantities associated with the flow are illustrated in Fig. 1. The origin of coordinates in the $z = x + iy$ plane is taken at the stagnation point on the wetted surface of the hydrofoil. This point is denoted by 0 in Fig. 1. The chordline of the profile is inclined at the angle α with respect to the x axis and the free-stream velocity U is taken as being parallel to this axis as illustrated. The flow separation point at or near the profile nose is the point A_1 as illustrated for a sharp-nosed foil. The "upper" cavity surface is shown as the dashed curve extending from A_1 to the point $0'$ at downstream infinity. In the case of a round-nose profile, A_1 can lie on the upper wetted surface behind the leading edge. This case is not illustrated in Fig. 1. The point A_2 denotes the location of the trailing edge of the wetted surface. The lower surface of the cavity leaves the wetted surface at A_2 and extends as shown by the dashed line to the point $0'$ at downstream infinity.

Let the coordinates of a typical point on the wetted surface be denoted by $\bar{x}$ and $\bar{y}$ and those on the upper cavity by x_c and y_c as shown in Fig. 1. While the orientation of the profile in the z plane is convenient for the purposes of analysis, the x-y system is not always a convenient reference frame for foil and cavity contours. For this purpose we use a coordinate system with the abscissa along the chordline as shown by the distance σ measured from the profile nose. The ordinates of the wetted surface are then given in terms of σ as $\eta(\sigma)$ and the upper cavity ordinates are given by $\eta_c(\sigma)$. At the trailing edge of the profile, the cavity thickness is $\eta_c = T$. These quantities are also shown in Fig. 1. In the σ,η system the stagnation point 0 is located at (σ_o,η_o) as illustrated. The transformation between the (x,y) and (σ,η) systems is

$$\sigma + i\eta = \sigma_o + i\eta_o + ze^{i\alpha} \quad , \tag{1}$$

where z is the complex variable, $z = x + iy$, and α is the angle-of-attack as measured by the inclination of the chordline with respect to the x axis and free-stream velocity U.

The conformal mappings start with the complex potential in the z-plane,

$$F = \phi + i\psi \quad , \tag{2}$$

where ϕ is the velocity potential and ψ is the stream function. As is customary, we adjust these quantities to make $\phi = 0$ at the stagnation point, 0. The stream function is taken to be zero all along the stagnation streamline. Therefore, the boundaries of the flow can be represented by a cut all along the real axis in the F-plane as shown in Fig. 2. Note that the wetted surface extends from the stagnation point

at 0 to the trailing edge at A_2 and the lower cavity surface from A_2 to $0'$ must lie along the lower surface of the cut. This is so because downstream from the stagnation point, the velocity potential increases in the flow direction and the stream function decreases outwardly from the foil or cavity surface. On the arc OA_1, the flow direction is reversed with a consequent reversal in the gradients of ϕ and ψ so that the point A_1 is on the upper edge of the cut.

One can use the mapping,

$$W = \sqrt{F} \tag{3}$$

in order to map the F-plane outside the cut into the upper half of the W-plane. Corresponding points are shown by the locations of $0'$, A_1 and A_2 and $0'$ in Fig. 3. As before, the cavity surfaces are shown as dashed lines and the wetted surface is shown by the solid line. Let the values of ϕ at A_1 and A_2 in the F-plane be ϕ_1 and ϕ_2 respectively. Then these points are at $W = \sqrt{\phi_1}$ and $W = -\sqrt{\phi_2}$ and the midpoint of the distance between A_1 and A_2 is located at

$$W = a = \frac{\sqrt{\phi_1} - \sqrt{\phi_2}}{2} \quad . \tag{4}$$

The distance between this midpoint and A_1 is

$$b = \frac{\sqrt{\phi_1} + \sqrt{\phi_2}}{2} \quad . \tag{5}$$

These distances are also shown in Fig. 3.

One can now use the mapping

$$W = \frac{\sqrt{\phi_2} - \sqrt{\phi_1}}{2} (Z + \cos \gamma) \quad , \tag{6}$$

where

$$\cos \gamma = \frac{a}{b} = \frac{\sqrt{\phi_1} - \sqrt{\phi_2}}{\sqrt{\phi_2} + \sqrt{\phi_1}} \quad , \tag{7}$$

in order to map A_1 into $Z = +1$ and A_2 into $Z = -1$. The point O maps into $Z = \cos \gamma$ as shown in Fig. 4. The significance of the point C, also shown in this figure, is discussed later. Then the Joukowski transformation,

$$Z = -\frac{1}{2} \left(\zeta + \frac{1}{\zeta}\right) \quad , \tag{8}$$

maps the upper half of the Z-plane onto the interior of the unit circle in the ζ-plane. The inverse of this mapping must be

$$\zeta = -Z + \sqrt{Z^2 - 1} \tag{9}$$

in order to make the point O' map into the origin of the ζ-plane. Various corresponding points are denoted by A_1, A_2 and O in Fig. 5. The arc of the unit semi-circle corresponds to the wetted surface. Coordinates on the wetted surface are given by $\zeta = e^{i\beta}$ as shown. The stagnation point is at $\beta = \gamma$. The upper surface of the cavity is on the real axis between A_1 and O' and the lower surface of the cavity is on the real axis between A_2 and O' as marked in Fig. 5. One can now use Eqs. (3) through (8) in order to write the composite of the preceding mappings as

$$F = b^2\left[\cos\gamma - \frac{1}{2}\left(\zeta + \frac{1}{\zeta}\right)\right]^2 \quad . \tag{10}$$

Then we introduce the complex velocity,

$$w = u - iv = \frac{dF}{dz} \quad , \tag{11}$$

in order to write

$$w = qe^{-i\theta} = b^2\left[\cos\gamma - \frac{1}{2}\left(\zeta + \frac{1}{\zeta}\right)\right]\left(-\zeta + \frac{1}{\zeta}\right)\frac{1}{\zeta}\frac{d\zeta}{dz} \quad , \tag{12}$$

or

$$wdz = dF = b^2\left[\frac{1}{2}\left(\zeta + \frac{1}{\zeta}\right) - \cos\gamma\right]\left(\zeta - \frac{1}{\zeta}\right)\frac{d\zeta}{\zeta} \quad . \tag{13}$$

These quantities are now used to define the logarithmic hodograph or ω-plane:

$$e^{-i\omega(\zeta)} = \frac{1}{U}\frac{dF}{dz} = \frac{w}{U} = \frac{q}{U}e^{-i\theta} = \exp\left[\ell n\,\frac{q}{U} - i\theta\right] \quad . \tag{14}$$

Therefore we have

$$\omega(\zeta) = \theta + i\ell n\,\frac{q}{U} = \theta + i\tau \quad , \tag{15}$$

where $\tau = \ell n\,\frac{q}{U}$. On the free streamlines $q = U$ so that $\tau = 0$ there. In the ζ-plane, these free streamlines are on the real axis and at $0'$ we know that $\theta = 0$ also. Therefore,

$$\omega(0) = 0 \tag{16}$$

and $\omega(\zeta)$ is real when ζ is real. At the stagnation point $q \to 0$ so that $\tau \to -\infty$ there. The flow directions differ by π on either side of 0 and so the ω-plane with the various corresponding boundaries can be represented as illustrated schematically in Fig. 6.

We can now use Eqs. (13), (14) and (15) in order to write

$$dz = dx + i dy = \frac{b^2 e^{-\tau+i\theta}}{U}\left[\frac{1}{2}\left(\zeta + \frac{1}{\zeta}\right) - \cos\gamma\right]\left(\zeta - \frac{1}{\zeta}\right)\frac{d\zeta}{\zeta} \quad . \tag{17}$$

On the wetted surface $\zeta = e^{i\beta}$ and Eq. (17) leads to

$$\left.\begin{aligned} d\bar{x} &= \frac{2b^2}{U} e^{-\tau}\left[\cos\gamma - \cos\beta\right]\sin\beta\cos\theta\, d\beta \\ \text{and} \\ d\bar{y} &= \frac{2b^2}{U} e^{-\tau}\left[\cos\gamma - \cos\beta\right]\sin\beta\sin\theta\, d\beta \end{aligned}\right\} \quad . \tag{18}$$

Note that $d\bar{y}/d\bar{x} = \tan\theta$ as it should if the wetted surface is to be a streamline. On the upper surface of the cavity $\tau = 0$ and $\arg\zeta = \pi$ so that Eq. (17) leads to

$$\left.\begin{aligned} dx_c &= \frac{b^2}{U}\cos\theta\left[\frac{1}{2}\left(\zeta + \frac{1}{\zeta}\right) - \cos\gamma\right]\left(\zeta - \frac{1}{\zeta}\right)\frac{d\zeta}{\zeta} \\ dy_c &= \frac{b^2}{U}\sin\theta\left[\frac{1}{2}\left(\zeta + \frac{1}{\zeta}\right) - \cos\gamma\right]\left(\zeta - \frac{1}{\zeta}\right)\frac{d\zeta}{\zeta} \end{aligned}\right\} \tag{19}$$

provided that $-1 \leq \xi \leq 0$.

Returning to Eq. (17), we can write the square of the arc length along the wetted surface as

$$(ds)^2 = dz\, d\bar{z} = \left\{2\frac{b^2}{U} e^{-\tau}\left[\cos\gamma - \cos\beta\right]\sin\beta\, d\beta\right\}^2 \quad ,$$

where we have also made use of Eq. (18) because it applies to the wetted surface. But from Eq. (15) we have

$$\tau = \ell n \frac{q}{U} = \ell n \sqrt{1 - C_p} \quad ,$$

so that

$$ds = 2 \frac{b^2}{U} [(\cos \gamma - \cos \beta) \sin \beta / \sqrt{1 - C_p(\beta)}] d\beta \qquad (20)$$

on the wetted surface of the profile. As we have noted previously, the flow directions differ by π on either side of 0. Therefore, if the sign of dz is positive on the arc $0A_2$, it will be negative along arc $0A_1$. As a result of this difference ds might have a like sign change in these two regions. Just how this might occur depends on the form of $\sqrt{1 - C_p(\beta)}$ in any particular case. Therefore, we will defer consideration of this question to a later place in the development.

Hydrodynamic Forces

The development of general formulae for the hydrodynamic forces on the profile depend upon certain properties of the function $\omega(\zeta)$ which result from the previously noted fact that $\omega(\zeta)$ is real when ζ is real. For then one can apply Schwartz's principle of symmetry in order to write $\omega(\bar{\zeta}) = \overline{\omega(\zeta)}$ and thereby obtain the analytic continuation of $\omega(\zeta)$ into the lower half of the unit circle [6]. Thus we can write for a prescribed modulus,

$r_0 = |\zeta| < 1$,

$$\theta(\beta) - i\tau(\beta) = \theta(-\beta) + i\tau(-\beta) \quad ,$$

or

$$\tau(-\beta) = -\tau(\beta)$$

and

$$\theta(-\beta) = \theta(\beta) \quad .$$

Hence τ is an odd function of β, or Im ζ, and θ is an even function of β, or Im ζ.

Using the result,

$$e^{\tau} = \sqrt{1 - C_p} \tag{21}$$

as noted above, and the fact that $\omega(\zeta)$ is now defined inside the unit circle one finds [7] from the calculus of residues that

$$C_L = \frac{\pi}{2} \frac{b^2}{Uc} \left[4\omega'(0) \cos \gamma - \omega''(0)\right] \tag{22}$$

and

$$C_D = \frac{\pi}{2} \frac{b^2}{Uc} \left[\omega'(0)\right]^2 \quad , \tag{23}$$

where the quantity c is the profile chord which is taken as unity in this work. The moment can be calculated after the complete solution has been found.

The Form of $\omega(\zeta)$ Near the Stagnation Point

This is also a well known result which we shall review briefly. The form of ω near 0 is dominated by the fact that on a smooth contour ω jumps by the amount π. In particular, as one traces the profile surface, starting at A_1 in Fig. 1 and then passes through 0 while proceeding to A_2, the jump is a decrease in θ. This is precisely the behavior exhibited by the real part of the analytic function $i\ell n(\zeta - e^{i\gamma})$. However this function by itself does not have the proper symmetry needed for admissible forms of ω. But if we subtract from it a similar function which has a like jump at the image of 0 with respect to the real axis in the ζ-plane, we preserve the necessary

behavior at 0 and also satisfy the preceding symmetry requirements. Aside from arbitrary additive constants, this function has the form

$$i\ell n \frac{\zeta - e^{i\gamma}}{\zeta - e^{-i\gamma}} .$$

Finally, we require the $\omega(0) = 0$. Because of this condition the resulting function which provides the flat plate solution is [4]

$$\omega_o(\zeta) = \theta_o + i\tau_o = -\alpha + i\ell n \frac{\zeta - e^{i\gamma}}{1 - \zeta e^{i\gamma}} , \qquad (24)$$

with $\gamma = \pi - \alpha$ in the case of an isolated flat-plate profile. For this case, one can show that this function has the flow direction, $\theta_o = -\alpha$ behind the stagnation point or $\theta_o = \pi - \alpha$ ahead of the stagnation point on $\zeta = e^{i\beta}$. Therefore, the wetted surface in the z-plane is a straight line through 0 with its trailing edge inclined at the angle $-\alpha$ with respect to the positive real axis. Moreover, since τ_o vanishes on the real axis in the ζ-plane, the free streamlines have $C_p = 0$ as required. Thus we can write Eq. (24) as

$$\omega_o(\zeta) = \pi H(\beta - \gamma) - \alpha + i\ell n \left| \frac{\zeta - e^{i\gamma}}{1 - \zeta} \right| , \qquad (24a)$$

where

$$H(\beta - \gamma) = \begin{cases} 0 , & \beta < \gamma \\ 1 , & \beta > \gamma \end{cases}$$

is the Heaviside function.

The contribution of ω_o to C_L and C_D follows from Eqs. (22) and (23). From Eqs. (22), (23) and (24) we get

$$C_{L_o} = 2\pi \frac{b^2}{Uc} \sin \alpha \cos \alpha \tag{25}$$

$$C_{D_o} = 2\pi \frac{b^2}{Uc} \sin^2 \alpha \tag{26}$$

and we see that $L/D = \cot \alpha$ as is proper for the flat plate. We can also use the relationship $C_p = 1 - e^{2\tau}$ to find the pressure distribution on the plate. The result is

$$C_{p_o} = \frac{4 \sin \beta \sin \gamma}{(\cos \beta - \cos \gamma)^2 + (\sin \beta + \sin \gamma)^2} \ . \tag{27}$$

From this result, we see that when $\beta = \gamma$, $C_{p_o} = 1$ and when $\beta = 0$ or π, $C_{p_o} = 0$ as required.

Continuing the study of the flat-plate solution, we can rewrite Eq. (24) for points on the wetted surface as

$$\omega_o = \pi - \alpha + \gamma + i\ell n[(e^{i\gamma} - e^{i\beta})/(e^{-i\gamma} - e^{i\beta})] \ ,$$

in which case

$$e^{\tau_o} = \left| \frac{e^{i\gamma} - e^{i\beta}}{e^{-i\gamma} - e^{i\beta}} \right| = \sqrt{1 - C_{p_o}} \ .$$

After some manipulation we find that

$$\sqrt{1 - C_{p_o}} = \frac{2|\cos \beta - \cos \gamma|}{(\cos \gamma - \cos \beta)^2 + (\sin \gamma + \sin \beta)^2} \quad .$$

Next we can put $\beta = \pi - \xi$ and $\gamma = \pi - \alpha$ in this expression and in Eq. (17) when it is written for points on the wetted surface. That is,

$$dz = -\frac{b^2}{U} \frac{(\cos \xi - \cos \alpha)}{|\cos \xi - \cos \alpha|} e^{i\theta}[(\cos \xi - \cos \alpha)^2 + (\sin \xi + \sin \alpha)^2]\sin \xi \, d\xi$$

$$= -e^{i\theta} \operatorname{sgn}(\cos \xi - \cos \alpha) \, 2 \frac{b^2}{U} [\sin \xi + \sin \alpha \sin^2 \xi - \cos \alpha \cos \xi \sin \xi] d\xi \quad .$$

We can dispose of the product $-e^{i\theta}$ sgn $(\cos \xi - \cos \alpha)$ by observing that on the wetted surface when $0 \leq \xi \leq \alpha$ the flow direction is $\theta = \pi - \alpha$ and when $\alpha \leq \xi \leq \pi$, $\theta = -\alpha$. Therefore in the first of these cases, $e^{i\theta} = -e^{-i\alpha}$ and in the second $e^{i\theta} = +e^{-i\alpha}$. Hence in either of them the product $-e^{i\theta}$ sgn $(\cos \xi - \cos \alpha) = e^{-i\alpha}$. Next we can introduce $d(\sigma + i\eta) = e^{i\alpha} dz$ from Eq. (1) with the result that

$$d(\sigma + i\eta) = 2 \frac{b^2}{U} [\sin \xi + \sin \alpha \sin^2 \xi - \cos \alpha \cos \xi \sin \xi] d\xi \quad .$$

This last result implies that $\eta = 0$ as is proper for a flat plate and $d\sigma$ is simply the arc length ds along the wetted surface measured from the profile nose where $\sigma = 0$. We can integrate this last equation from $\sigma = 0$ $(\xi = 0)$ to some value, $0 \leq \sigma \leq 1$ $(0 \leq \xi \leq \pi)$, and get

$$s = 2 \frac{b^2}{U} \left[(1 - \cos \xi)\left(1 - \frac{\cos \alpha}{2} [1 + \cos \xi]\right) + (\xi - \sin^2 \xi) \frac{\sin \alpha}{2}\right] \quad . \qquad (28)$$

The profile is to have unit chord however, so that when $\xi = \pi$, $\sigma = s = 1$ and

$$\frac{b^2}{U} = \frac{1}{4 + \pi \sin \alpha} \quad . \tag{29}$$

When Eq. (29) is used in Eqs. (25) and (26), one obtains the well known Rayleigh formulae [12].

Additional properties of the flat-plate solution which are important for the present considerations relate to the shape of the upper surface of the cavity. In Fig. 5, ζ will be on the negative real axis for points on this part of the cavity. Therefore, let us put $\zeta = -\zeta_c$ where ζ_c is a real positive number. Then we can use $d(\sigma + i\eta) = e^{i\alpha} dz$, and write Eq. (17) in the form

$$d(\sigma + i\eta) = \frac{b^2}{U} \exp i[\alpha + \theta_o(\zeta_c)] d\{[\tfrac{1}{2}(\zeta_c + \frac{1}{\zeta_c}) - \cos \alpha]^2\} \quad .$$

But now

$$\exp i[\alpha + \theta_o] = e^{-i\alpha}(e^{i\alpha} - \zeta_c)/(e^{-i\alpha} - \zeta_c)$$

and so we have

$$d(\sigma + i\eta) = \frac{1}{2} \frac{b^2}{U} [\zeta_c e^{-i\alpha} - 2 + (2i \sin \alpha)/\zeta_c + 2/\zeta_c^2 - e^{i\alpha}/\zeta_c^3] d\zeta_c \quad .$$

The integration in this case starts at A_1 where $\zeta_c = 1$ and $\sigma = \eta = 0$ and proceeds to some value of σ_c, η_c corresponding to $1 \leq \zeta \leq 0$. This leads to the parametric representation of $\eta_c(\sigma_c)$ in terms of ζ_c which is given by

$$\sigma_c = \frac{1}{2}\frac{b^2}{U}\frac{(1-\zeta_c)^2}{\zeta_c}\left[\frac{(1+\zeta_c)^2}{2\zeta_c}\cos\alpha - 2\right] \tag{30}$$

and

$$\eta_c = \frac{1}{2}\frac{b^2}{U}\sin\alpha\left[\frac{1-\zeta_c^4}{2\zeta_c^2} + 2\,\ell n\zeta_c\right] \tag{31}$$

Equation (29) gives the value of $\frac{b^2}{U}$ to be used in Eqs. (30) and (31).

It is useful to find the ordinate of the upper surface of the cavity above the trailing edge of the wetted surface. This can be done by calculating the quantity

$$f(\zeta_c,\alpha) = \frac{(1-\zeta_c)^2}{\zeta_c}\left[\frac{(1-\zeta_c)^2}{2\zeta_c}\cos\alpha - 2\right]$$

for several values of ζ_c and prescribed values of α. Then when $\sigma_c = 1$, one can plot contours of α = constant in an $f - \zeta_c$ plane and note for each value of α the value of ζ_c corresponding to $f = 2(4 + \pi \sin\alpha)$. These values of ζ_c can then be used in Eq. (31) in order to compute the value of $\eta_c(1)$ for each value of α. It was found when these points were plotted in an $\eta_c(1) - \alpha$ plane that a linear relationship fits the data for $0 \leq \alpha \leq 10°$. When α is measured in degrees, this line has the equation

$$\eta_c(1) = .0294\alpha° \quad . \tag{32a}$$

The corresponding relationship for α measured in radians is

$$\eta_c(1) = 1.684\alpha \quad . \tag{32b}$$

The computed results are tabulated below.

Table 1. Cavity Thickness at the Trailing Edge of a Flat Plate

$\alpha°$	$\zeta_c(1)$	$\eta_c(1)$
0.0	-----	.0000
0.5	.1712	.0147
1.0	.1707	.0297
2.0	.1698	.0585
3.0	.1689	.0879
4.0	.1680	.1174
5.0	.1669	.1463
7.0	.1650	.2049
10.1	.1620	.2939

These results will be used in order to start the functional iteration after the formulation of the theory has been completed. As a final note, we observe that the cavity thickness at the trailing edge of a flat plate according to linearized theory [13] is

$$\eta_c(1) = 1.681\alpha \quad ,$$

which can be compared to the corresponding expression from Eq. (32b). Within the range of attack angles considered here the trailing-edge cavity thickness at zero cavitation number is about the same when estimated by linearized or nonlinear theory. For larger values of attack angle, we would expect estimates from linearized theory to exceed nonlinear cavity thicknesses.

The flat-plate function $\omega_o(\zeta)$ is traditionally considered to possess all of the singular behavior of the function $\omega(\zeta)$. The shape of the smooth body is then represented by an analytic function $\omega_1(\zeta)$ which is regular inside and on the unit circle. It must also satisfy the same symmetry requirements as are imposed upon ω_o and we must also insist that $\omega_1(0) = 0$. Then one traditionally puts $\omega(\zeta) = \omega_o + \omega_1$. As mentioned previously, we will add to this customary sum a new function, $\omega_c(\zeta)$, which is the analog of the point-drag function of linearized theory. We will now explore the properties of this eigensolution.

A Simple Eigensolution

The complementary function $\omega_c = \theta_c + i\tau_c$, is to be determined from the requirements that $\tau_c = 0$ on the cavity and the foil, $\theta_c = 0$ along the stagnation streamline and that ω_c vanishes at infinity. A function of the form which satisfies these conditions can be found most easily by considering the flow in the F-plane, Fig. 2. If we take

$$\omega_c = \theta_c + i\tau_c = \frac{E}{\sqrt{F}} \tag{33}$$

where E is a real constant, we have a function which satisfies the necessary requirements. The two conditions $\omega_c(\infty) = 0$ and $q_c = U$ on both the cavity and the profile wetted surface can be satisfied by any member of the family of functions having the form F^{-m}, $0 < m < 1$. But the condition $\theta_c = 0$ along the entire stagnation streamline can be satisfied only when $m = 1/2$. This choice for the complementary function seems to offer the advantage that it will cause less alteration of the upstream flow field inclination than other possibilities. Moreover, it is the only choice from amongst the functions F^{-m} which gives the correct branching of the flow and it appears to be the most convenient choice for further analysis. Consequently, we shall adopt this functional form for the simple eigensolution in this work. The word simple indicates that the branch point for this solution is coincident with the stagnation point at 0 in Fig. 1. We shall generalize this result later.

It has been noted by O. Furuya* that Eq. (33) is just the single-spiral-vortex function proposed by Tulin as a useful representation for cavity termination in the direct problem at non-zero cavitation numbers [14]. The small-scale structure of this function is responsible for its name as discussed by Tulin on p. 21 of Ref. [14]. In connection with the present application, we may also mention Tulin's double spiral vortex model [14] which we shall write as

$$\omega_{c_d} = \theta_{c_d} + i\tau_{c_d} = D \ln \sqrt{F} = D\left[\ln \sqrt{r} + i\left(\frac{\arg F}{2}\right)\right] ,$$

where D is a real constant and $r = |F|$. At points in the physical plane which are far removed from the profile and the cavity, $F \sim U_z$ and ω_{c_d} is not bounded at the point O'. As it stands, this form of the double-spiral vortex violates Eq. (16) and it will generally not produce a null pressure coefficient everywhere on the wetted surface. Therefore, it is not an admissible candidate for an eigenfunction. This is not to say that other logarithmic forms for an eigenfunction can not be acceptable. This writer has not found one as yet, however. Therefore, we shall content ourselves with the form of ω_c prescribed by Eq. (33) and restrict the present analysis to eigensolutions of this form.

Equation (10) can be used to represent ω_c in the ζ-plane as

$$\omega_c = \frac{E}{b\left[\cos\gamma - \frac{1}{2}\left(\zeta + \frac{1}{\zeta}\right)\right]} = \frac{-2E\zeta}{b(\zeta - e^{i\gamma})(\zeta - e^{-i\gamma})} . \qquad (34)$$

---

*Private Communication (March 1985).

In the ζ-plane $\omega_c(0) = 0$ and when ζ is real, ω_c is real. Moreover, $\omega_c(\zeta)$ is an analytic function which is regular inside the unit circle and which has simple poles at $\zeta = e^{\pm i\gamma}$. Note from Eq. (34) that on the "nose cavity" $\theta_c \to 0+$ as $\zeta \to -0$ and on the "tail cavity" $\theta_c \to 0-$ as $\zeta \to +0$, as illustrated in Fig. 1 also. From Eq. (14), $w_c = Ue^{-i\omega_c}$ and we see that the structure of ω_c leads to an essential singularity in w_c at the stagnation point 0. The complex velocity w_c is bounded at this point however*, and a smooth foil contour will pass through $z = 0$ as will be shown below. At points on the unit circle, $\zeta = e^{i\beta}$, we have

$$\tau_c = 0 \tag{35}$$

and

$$\theta_c(\beta) = \frac{E}{b[\cos\gamma - \cos\beta]} = \frac{-E}{2b \sin\frac{\gamma+\beta}{2} \sin\frac{\gamma-\beta}{2}} . \tag{36}$$

---

*For points on the unit circle very near the stagnation point, $\beta = \gamma$, let $\beta = \gamma - \varepsilon$ with $\varepsilon \ll 1$. Then

$$\omega_c(\gamma,\varepsilon) \doteq \frac{E}{\varepsilon b[\sin\gamma + \frac{\varepsilon}{2}\cos\gamma]}$$

and to $O(\varepsilon^{-1})$ $w_c \doteq \exp - iE/\varepsilon b \sin\gamma$. Therefore $|w_c| = q_c < 1$ as $\varepsilon \to 0$. Next consider an interior point, $\zeta = re^{i\gamma}$. Now let $r = 1 - \rho$ with $0 < \rho \ll 1$. Then to $O(\rho^{-1})$, $\omega_c(\gamma,\rho) = \frac{-iE}{\rho b \sin t} = i\ell nq_c/U$. Consequently, $q_c/U = \exp - E/\rho b \sin\gamma$ and $q_c/U \to 0$ as $\rho \to 0$. Appropriate linear combinations of these two cases can be used to consider other limiting paths but these give no new information about the boundedness of q_c/U.

Since $\tau_c = 0$ on the wetted surface, we expect ω_c to make no contribution to the lift although the singularity at the stagnation point should lead to a drag force. Making use of Eqs. (22), (23) and (34), we find that

$$C_{L_c} = 0$$

and

$$C_{D_c} = 2\pi \frac{E^2}{Uc} \quad .$$

From Eq. (36) we see that the flow direction is not defined at the stagnation point, $\beta = \gamma$. If $\beta < \gamma$ however,

$$\theta_c = -\frac{E}{b[\cos \beta - \cos \gamma]} < 0$$

along the arc OA_2. If $\beta > \gamma$

$$\theta_c = \frac{E}{b[\cos \gamma - \cos \beta]} > 0 \quad ,$$

along the arc OA_1. Therefore θ_c changes sign at $\beta = \gamma$ and as noted previously, the real part of ω_c has a jump of π as it passes through 0. In view of Eq. (15) which requires that $\tau = \ell nq/U$, this situation suggests a strong similarity between Fabula's "step-profile" solution for the linearized theory [15] and the present eigensolution. The present application and those of Refs. [13] and [15] are different, however.

Simple Eigensolution Geometry

The shape of the wetted and cavity surfaces follows from the relationships of Eq. (14) which can be expressed as

$$dz = \frac{dF}{U} e^{i\omega_c} = \frac{d(\sqrt{F}^2)}{U} e^{iE/\sqrt{F}} \quad .$$

If we put $t = E/\sqrt{F}$, we find for a profile of unit chord that

$$dz = -\frac{2E^2}{U}\frac{1}{t^3}e^{it}dt = -\frac{C_{D_c}}{\pi}\frac{1}{t^3}d^{it}dt$$

which has the indefinite integral,

$$z = \frac{E^2}{U}\left\{\frac{e^{it}}{t^2} + i\,\frac{e^{it}}{t} + \int \frac{e^{it}}{t}\,dt\right\} \quad . \tag{37}$$

Completion of this integration can be carried out in four parts starting from either side of the stagnation point where $z = 0$ and $t \to \infty$.

For example, on the arc OA_1 we recall that $\beta > \gamma$. Put $t = t_1$, $\gamma = \pi - \delta$ and $\beta_1 = \pi - \xi_1$ then

$$t_1 = \frac{E}{b(\cos\,\xi_1 - \cos\,\delta)} \quad .$$

Because $0 < \xi_1 < \delta$, we have

$$\frac{E}{b(1 - \cos\,\delta)} < t_1 < \infty \quad .$$

After separating Eq. (37) into real and imaginary parts, we find for this part of the wetted surface, the coordinates

$$\left.\begin{aligned} x_1 &= \frac{E^2}{U}\left[\frac{\cos\,t_1}{t_1^2} - \frac{\sin\,t_1}{t_1} + Ci(t_1)\right] \\ \text{and} \qquad y_1 &= \frac{E^2}{U}\left[\frac{\sin\,t_1}{t_1^2} + \frac{\cos\,t_1}{t_1} + Si(t_1) - \frac{\pi}{2}\right] \end{aligned}\right\} \quad . \tag{38}$$

On the rest of the wetted surface, that is, on arc OA_2 between the stagnation point and the tail, we know that $\beta < \gamma$ and we put $t = -t_2$, $\gamma = \pi - \delta$ and $\beta_2 = \pi - \xi_2$. Then

$$t_2 = \frac{E}{b[\cos\delta - \cos\xi_2]} .$$

In this case, $\delta < \xi_2 < \pi$ and it follows that

$$\infty < t_2 < \frac{E}{b(1 + \cos\delta)} .$$

Then we have

$$\left.\begin{aligned} x_2 &= \frac{E^2}{U}\left[\frac{\cos t_2}{t_2^2} - \frac{\sin t_2}{t_2} + C_i(t_2)\right] \\ \text{and} \qquad y_2 &= -\frac{E^2}{U}\left[\frac{\sin t_2}{t_2^2} + \frac{\cos t_2}{t_2} + Si(t_2) - \frac{\pi}{2}\right] \end{aligned}\right\} . \qquad (39)$$

On the cavity surface A_1O' the integration starts at $\zeta = -1$ and ends somewhere between $\zeta = -1$ and $\zeta = 0$. Note that the value of t at $\zeta = -1$ equals that of t_1 when $\beta = 0$. So that if we put $t = t_3$, $\gamma = \pi - \delta$ and $\zeta = -\zeta_3$, we have

$$t_3 = \frac{E}{b[\frac{1}{2}(\zeta_3 + \frac{1}{\zeta_3}) - \cos\gamma]} ,$$

then the upper cavity joins the nose arc of the wetted surface and its coordinates are

$$\left.\begin{aligned} x_3 &= \frac{E^2}{U}\left[\frac{\cos t_3}{t_3} - \frac{\sin t_3}{t_3} + Ci(t_3)\right] \\ \text{and} \\ y_3 &= \frac{E^2}{U}\left[\frac{\sin t_3}{t^3} + \frac{\cos t_3}{t_3} + Si(t_3) - \frac{\pi}{2}\right] \end{aligned}\right\} . \qquad (40)$$

In this case

$$0 < t_c \leq \frac{E}{b(1 - \cos \delta)} .$$

Finally, the cavity surface from the trailing edge is obtained by putting $t = - t_4$, $\gamma = \pi - \delta$ and $\zeta = \zeta_4$, where $0 \leq \zeta_4 \leq 1$. Therefore

$$t_4 = \frac{E}{b[\cos \delta - \frac{1}{2}(\zeta_4 + \frac{1}{\zeta_4})]}$$

and

$$0 < t_4 \leq \frac{E}{b(1 + \cos \delta)} .$$

Then we have

$$\left.\begin{aligned} x_4 &= \frac{E^2}{U}\left[\frac{\cos t_4}{t_4^2} - \frac{\sin t_4}{t_4} + C_i(t_4)\right] \\ \text{and} \\ y_4 &= -\frac{E^2}{U}\left[\frac{\sin t_4}{t_4^2} + \frac{\cos t_4}{t_4} + Si(t_4) - \frac{\pi}{2}\right] \end{aligned}\right\} . \qquad (41)$$

As we found for the upper cavity, the lower cavity surface starts smoothly from the wetted surface.

Equations (38), (39), (40) and (41) will provide the shape of the wetted surface and the cavity surfaces for the simple complementary function of Eq. (34). These equations contain the undetermined ratio E^2/U, however. We shall consider the ratio E/b, which determines the strength of the complementary solution, as a parameter which we can prescribe -- at least for the time being. We also consider the value of γ (or δ) to be known. Therefore, we need to "scale" our results in order to obtain a profile of unit chord. Since we anticipate that the complementary function can produce a rounding of the wetted surface nose, the scaling procedure must account for this possibility. Accordingly, we shall need to determine explicitly the location of the apex of the wetted surface nose with respect to the profile chordline.

Figure 1 shows the chordline for the sharp-nose or for the round-nose case when the upper cavity separates at the leading edge with respect to the hydrofoil chord. The geometry for the rounded nose with the separation point on the upper wetted surface behind the apex of the wetted surface contour is illustrated in Fig. 7. The apex is located at the origin of σ, η coordinates in this illustration with the η axis being tangent to the contour at this point. Denote the x, y coordinates of this point by x_a, y_a. Then since the σ-axis is normal to the η axis, we see that at the apex the slope of the contour is

$$\frac{dy_a}{dx_a} = \tan\left(\frac{\pi}{2} - \alpha\right) = \cot\alpha \quad . \tag{42}$$

We will restrict our attention to those cases in which the apex is on the arc OA_1. Let $t = t_1 = t_a$ at the apex. Then from the equations preceding Eq. (38), which define t_1, we have

$$t_a = \frac{E}{b(\cos \xi_a - \cos \delta)} \quad , \quad 0 < \xi_a < \delta \quad , \tag{43}$$

and Eq. (43) can then be used in Eqs. (38) to define x_a and y_a once the value of ξ_a (or β_a) has been found. Thus, we must determine the unknowns E^2/U and ξ_a in terms of the prescribed quantities E/b and δ(or γ). Two conditions are available for this purpose. The first is given by Eq. (42). The second will be that the profile has a unit chord.

An alternate form of Eq. (42) is

$$\cos \alpha = \sin t_a$$

and $$\tag{44}$$

$$\sin \alpha = \cos t_a$$

which follows from the complex equation just above Eq. (37) when we put $t = t_a$. We will use Eq. (43) as the appropriate expression for the slope of the foil contour at the apex. Now let us differentiate Eq. (1) so that

$$d(\sigma + i\eta) = e^{i\alpha} dz \quad .$$

Then from the complex equation just preceding Eq. (37) we have

$$e^{-i\alpha} d(\sigma + i\eta) = -\frac{2E^2}{U} \frac{1}{t^3} e^{it} dt \quad . \tag{45}$$

Starting from 0 where $(\sigma,\eta) = (\sigma_o,\eta_o)$, we integrate Eq. (45) to A_2, where $(\sigma,\eta) = (1,0)$. This step gives

$$e^{-i\alpha}(1 - \sigma_o - i\eta_o) = \frac{E^2}{U}\left\{\left[\frac{\cos t_t}{t_t^2} - \frac{\sin t_t}{t_t} + Ci(t_t)\right]\right.$$

$$\left. - i\left[\frac{\sin t_t}{t_t^2} + \frac{\cos t_t}{t_t} + Si(t_t) - \frac{\pi}{2}\right]\right\} ,$$

where

$$t_t = \frac{E}{b(1 + \cos \delta)} ,$$

corresponding to t_2 with $\xi_2 = \pi$ in Eqs. (39). Next we can use Eqs. (38) with $\xi_1 = \xi_a$ and $t_1 = t_a$ or

$$t_a = \frac{E}{b(\cos \xi_a - \cos \delta)}$$

at the apex in order to integrate Eq. (45) from 0 to the apex along the arc OA_1. This step results in

$$- e^{-i\alpha}(\sigma_o + i\eta_o) = \frac{E^2}{U}\left\{\left[\frac{\cos t_a}{t_a^2} - \frac{\sin t_a}{t_a} + Ci(t_a)\right]\right.$$

$$\left. + i\left[\frac{\sin t_a}{t_a^2} + \frac{\cos t_a}{t_a} + Si(t_a) - \frac{\pi}{2}\right]\right\} .$$

Eliminating the sum $\sigma_o + i\eta_o$ from these two equations, we get

$$\left.\begin{aligned} \frac{U}{E^2}\cos\alpha &= F - f(t_a) \\ \text{and} \\ \frac{U}{E^2}\sin\alpha &= G - g(t_a) \end{aligned}\right\}. \qquad (46)^*$$

In Eqs. (46) we have

$$\left.\begin{aligned} F &= \frac{x_t U}{E^2} = \frac{\cos t_t}{t_t^2} - \frac{\sin t_t}{t_t} + Ci(t_t) \\ \text{and} \\ G &= \frac{y_t U}{E^2} = \frac{\sin t_t}{t_t^2} + \frac{\cos t_t}{t_t} + Si(t_t) - \frac{\pi}{2} \end{aligned}\right\} \qquad (47)$$

which contain known quantities because t_t is known. The remaining pair of functions,

$$\left.\begin{aligned} f(t_a) &= \frac{\cos t_a}{t_a^2} - \frac{\sin t_a}{t_a} + Ci(t_a) \\ \text{and} \\ g(t_a) &= \frac{\sin t_a}{t_a^2} + \frac{\cos t_a}{t_a} + Si(t_a) - \frac{\pi}{2} \end{aligned}\right\}, \qquad (48)$$

contains t_a which depends upon the unknown, $\beta_a = \pi - \xi_a$. Thus, Eqs. (46) are two simultaneous equations containing the quantities U/E^2, α and β_a which must be determined. Therefore, Eqs. (44) and (46) form a determinate system

---

*The F introduced here is not to be confused with $F = \phi + i\psi$ from Eq. (2).

which can be solved by iteration. In order to do this, we can write the complete system as

$$\tan \alpha = \frac{G - g(t_a)}{F - f(t_a)} \quad , \tag{49}$$

$$\cot t_a = \tan \alpha \tag{50}$$

and

$$\frac{U}{E^2} = \frac{F - f(t_a)}{\cos \alpha} = \frac{G - g(t_a)}{\sin \alpha} \quad . \tag{51}$$

In the derivation of this system we have assumed that the apex, z_a, is on the arc $0A_1$. On the other hand, we specify the quantities E/b and $\gamma = \pi - \delta$. We must now determine whether or not our assumption regarding the location of z_a can restrict possible choices for the parameters E/b and δ. In particular, we recall that, as is true for the quantity ξ_1, we must also require that $0 < \xi_a < \delta$, as noted in Eq. (45). The limiting condition, corresponding to the coincidence of the apex and cavity separation point at the nose of the profile corresponds to $\xi_a = 0$. In this case, the smallest value of t_1 for any choice of E/b will be found when

$$t_a\Big|_{min} = \frac{E}{b(1 - \cos \delta)} \quad .$$

On the other hand, by inspection of Eqs. (47) and (48), we see that the largest values of f and g are found for $t_a = t_{min}$. The values of F and G are also obtained from the smallest value of t_2 because t_t is calculated from t_2 with $\xi_2 = \pi$, namely:

$$t_t = \frac{E}{b(1 + \cos \delta)} \quad .$$

Let us compare the values of F with f and G with g. Suppose that E/b is selected so that $\cos t_a \approx \cos t_t \approx 1$, $\sin t_a \approx t_a$ and $\sin t_t \approx t_t$. Let $\delta << 1$. In this case we can see that

$$\frac{F}{f} = \left[\frac{t_a\Big|_{min}}{t_t}\right]^2 = \left(\frac{2}{\delta}\right)^4 \left[1 - \frac{2\delta^2}{3}\right] \quad \text{and} \quad \frac{G}{g} = \left[\frac{t_a\Big|_{min}}{t_t}\right] = \left(\frac{2}{\delta}\right)^2 \left[1 - \frac{\delta^2}{6}\right] \quad .$$

For example, if $\delta = .1$, we would estimate $F/f \sim (20)^4$ and $G/g \sim (20)^2$. These estimates imply that both E/b and δ are significantly smaller than unity. In the applications contemplated, E/b will probably be less than unity although δ might conceivably approach or exceed unity. Therefore, we shall consider the ratio,

$$\frac{t_a\Big|_{min}}{t_t} = n = \frac{1 + \cos \delta}{1 - \cos \delta} \quad , \quad n > 1 \quad ,$$

which permits us to consider roughly the ratios of F to f and of G to g for various values of δ. In particular, we can solve for $\cos \delta$ and obtain

$$\cos \delta = \frac{n - 1}{n + 1} \quad ,$$

which permits us to plot a curve of $n = \left(t_a\Big|_{min}/t_t\right)$ versus δ as shown in Fig. 8. This curve illustrates the effect that the choice of stagnation point location has on the ratio, n. The value of n in turn gives a rough indication of how large the ratios F/f and G/g will be.

It appears for most cases that these ratios will be very large and one need not solve Eqs. (49) and (50) by iteration. Instead one can obtain an accurate value of α from

$$\tan \alpha \triangleq \frac{G}{F} \tag{49a}$$

and he can then determine U/E^2 from

$$\frac{U}{E^2} = \frac{F}{\cos \alpha} \quad . \tag{51a}$$

Should cases arise in which Eqs. (49a) and (51a) are not accurate, they can be used advantageously to start the iteration. In order to illustrate these points and in order to show a profile shape derived from the complementary solution, we have prepared the following numerical example.

We started the calculation by selecting $\delta = 70°$ and $E/b = .01$. Figure 8 shows that $n \triangleq 2$. The values $t_a\Big|_{min} = .01520$ and $t_t = .00745$ follow from the formulae for these quantities. From Eqs. (47) we find that $F = 18{,}004$ and $G = 266.83$. Equations (49a) and (51a) lead to $\tan \alpha = .01482$ and $U/E^2 = 18{,}006$. From the formulae just after Eq. (36) we have for the cavity drag due to a profile of unit chord

$$C_{D_c} = 2\pi \frac{E^2}{U} = .00035$$

as the contribution for this point-drag profile. The value of t_a can now be found from Eq. (50). It is $t_a = 1.556$. Equation (43) can now be used to find that $\xi_a = 69.61°$. Note that for this case the apex is almost coincident with the stagnation point. Because Eq. (35a) shows the

complementary function to be at the stagnation point this result is expected. The fact that the apex is not exactly at $\delta = 70°$ is due only to the inclination, $\alpha = .85°$, between the chord line and the x axis. Once U/E^2 has been found, the values of x_t and y_t can be found from Eqs. (47). The values are $x_t = .99989$ and $y_t = -.01482$. Now one can use the conditions that in Eqs. (1), $(x_t, y_t) \leftrightarrow (\sigma=1, \eta=0)$ and $(x_a, y_a) \leftrightarrow (\sigma=0, \eta=0)$. These lead to a system of equations from which σ_o and η_o can be eliminated and one finds that

$$x_a = x_t - \cos \alpha = x_t - \sin t_a \quad ,$$

$$y_a = y_t + \sin \alpha = y_t + \cos t_a \quad .$$

When the above values of x_t and α were used in these equations, the values of x_a and y_a were found to be zero to within five decimal places. This result is consistent with the location of ξ_a noted previously. Continuing with Eqs. (1), we can use the fact that $x_a = y_a = 0$ to see that it must also follow that $\sigma_o = \eta_o = 0$. Accordingly, the form of Eqs. (1) for the present calculations is

$$\sigma = .99989x - .014796y \quad ,$$

$$\eta = .014796x + .999989y \quad .$$

The next phase of the calculations is the evaluation of the equations for the wetted surface and cavity contours in accordance with Eqs. (38), (39) and (40). The result of these calculations is shown in Fig. 9. In this figure, the chordline distance, σ, has been labeled as X and the ordinate, η, has been labeled as Y. Note that the Y-scale is magnified five times compared to that of the X-scale. The trailing edge of the

wetted surface is at X = 1. The upper surface separation point is at $\sigma = X = .240$. The cavity thickness at X = 1 is Y = T = .02980. This point is marked to the same scale as the X-scale by the dot and the line at X = 1 in order to give an idea of the actual thickness of this example of a point-drag profile. Finally we can calculate the value of $\zeta_c(1)$ in this example in order to compare it with the values found previously for the flat-plate. It is found from the value of $t_c = (E/b)/[(\zeta_c + 1/\zeta_c)/2 \cos \gamma]$ at $\sigma = 1$. The calculations indicated give $\zeta_c(1) = .3290$ which is roughly two times the value from Table 1.

The Eigensolution

Our desire to retain as much simplicity as possible in the preceding analysis of the complementary function has caused us to place the point-drag singularity at the stagnation point, and that is why we call it the simple eigensolution. This restriction on the location of the point of application has allowed us to show that such a solution exists, that it definitely leads to a smoothly rounded profile nose and that it will cause an incremental thickening of the cavity depending on its strength, E. Of course, we need not restrict ourselves to the stagnation point as being the location of the point-drag singularity.

For example, suppose we choose some other point C on the wetted surface. Such a point is illustrated in Fig. 5 and it happens to be located between the upper cavity separation point and the stagnation point, although C could just as well be at some other wetted-surface location. The main idea is that now $\beta = \gamma_c$ at the location of the point-drag singularity and if we simply replace Eq. (34) by the modified expression,

$$\omega_c(\zeta) = \frac{E}{b[\cos \gamma_c - \frac{1}{2}(\zeta + \frac{1}{\zeta})]} = \frac{-2E\zeta}{b(\zeta - e^{i\gamma_c})(\zeta - e^{-i\gamma_c})}$$

$$= \frac{iE}{b \sin \gamma_c}\left[\frac{e^{i\gamma_c}}{\zeta - e^{i\gamma_c}} - \frac{e^{-i\gamma_c}}{\zeta - e^{-i\gamma_c}}\right] , \qquad (34a)$$

we still have a function which satisfies those conditions needed for a complementary solution. It is clear that in the ζ-plane, $\omega_c(0) = 0$ is in agreement with Eq. (16). Moreover, when ζ is real ω_c is real and on the unit circle $\tau_c = 0$ everywhere except possibly at the simple poles, $\zeta = e^{\pm i\gamma_c}$. From Eqs. (22) and (23) it follows that

$$C_{D_c} = 2\pi \frac{E^2}{Uc} \qquad (52)$$

as before. On the other hand, because of the displacement of the point C away from 0, a lift force is produced and we find that now

$$C_{L_c} = \frac{8\pi bE}{Uc} \sin \frac{\gamma + \gamma_c}{2} \sin \frac{\gamma - \gamma_c}{2} = \frac{8\pi bE}{Uc} \sin \frac{\delta_c + \delta}{2} \sin \frac{\delta_c - \delta}{2} , \qquad (53)$$

where $\gamma = \pi - \delta$ and $\gamma_c = \pi - \delta_c$ in accordance with previous convention. The profile chord, c, should be set at unity in Eqs. (52) and (53). Equation (53) shows that $C_L = 0$ when $\delta_c = \delta$. But $\delta_c < \delta$ when the point C moves toward the point A_1 and a negative lift results. In the limit as $\delta_c \to 0$, we have

$$C_{L_c} = -\frac{8\pi bE}{Uc} \sin^2 \frac{\delta}{2} .$$

If C is between 0 and A_2 a positive lift is produced and in the limit when C is coincident with A_2 we have

$$C_{L_c} = \frac{8\pi bE}{Uc} \cos^2 \frac{\delta}{2} \quad .$$

If one were to let E be negative the sign of the foregoing trends with respect to C_L would be reversed. We must insist however, that $E \geq 0$ because this function produces a thickening of the cavity and because then $\omega_c'(0) = -2E/b$. Similarly, we have also found that $\omega_o'(0) = -2 \sin \gamma$. Thus, the effect of adding ω_o and ω_c <u>increases</u> the net drag. Neither of these functions can act to reduce it. Accordingly, we shall take Eq. (34a) as the appropriate form of the eigensolution which has been sought. Since both of Eqs. (34) have simple poles on the contour $|\zeta| = 1$, they can be thought of as elementary solutions. But as we have seen in the case of the simple eigensolution, the pole at $\beta = \gamma_c$ does not lead to an unbounded value of q_c/U. Indeed, $0 \leq q_c/U \leq 1$ in the neighborhood of $\beta = \pm \gamma_c$, which can be taken to be at any point on the wetted surface when $\beta = + \gamma_c$.

<u>Some Profile Geometry and the Flow</u>

In any inverse design procedure, one starts the calculation by prescribing the pressure distribution or the magnitude of the velocity along the periphery of the profile. Of course, that is almost like having the solution at the outset; but not quite, because one does not know the relationship between points along the hydrofoil arc length, s, and corresponding points on the semi-circle in the ζ plane. Nevertheless, referring to Fig. 7, we can measure the arc length s from the point A_2 at the cavity-trailing edge separation point. Then the arc length increases from A_2 until one reaches the stagnation point 0 in

in Fig. 7. At 0 the arc length will be designated by s_o. Continuing along the periphery, one rounds the nose of the foil and arrives at the separation point A_1. At this point, the arc length is s_1. Finally we proceed along the upper surface of the cavity until we arrive at the point s_2, a distance T directly above the trailing edge, A_2. The distance T is measured perpendicularly to the profile chordline. Thus, it is parallel to the η axis in Fig. 7. Clearly, $0 < s_o < s_1 < s_2$.

A schematic diagram showing the flow speed on the wetted-surface arc and the upper surface of the cavity is illustrated in Fig. 10. This figure shows rather clearly that the designer does not have as much freedom with regard to the pressure distribution prescription as he might wish. For example, we know that $|q/U| = 1$ at $s = 0$, $s = s_1$ and in the interval, $s_1 \leq s \leq s_2$. Moreover we take the values of $q/U \leq 0$ in the interval $0 \leq s \leq s_o$ because the flow direction on the wetted surface points in the direction opposite to the positive sense of s. Between $s_o \leq s \leq s_2$ the opposite situation holds and we count $q/U \geq 0$ in this interval. At no point in the flow can $q/U > 1$.

Since we prescribe the magnitude of q/U everywhere this is the same as prescribing the lift coefficient C_L. The prescribed value of C_L can be used to fix the relative position of the stagnation point s_o with respect to point s_2 if the distribution q(s)/U is not too firmly fixed. One need only use the well-known Kutta-Joukowsky formula,

$$\frac{1}{2} cC_L = \frac{\Gamma}{U} = \int_0^{s_2} (q/U)ds \quad ,$$

where c is the profile chord and Γ is the circulation. But we can write

$$\Gamma = (\Delta_2 - \Delta_1)U \quad ,$$

where

$$\Delta_1(s_o) = \int_0^{s_o} \frac{q(s)}{U}\, ds$$

and

$$\Delta_2(s_o, s_2) = \int_{s_o}^{s_1} \frac{q(s)}{U}\, ds + (s_2 - s_1) \quad .$$

Generally one will need to solve for the ratios s_o/s_2 and s_1/s_2 numerically, starting the iteration by supposing that possibly Δ_1 and that part of Δ_2 between s_o and s_1 are triangular areas. Indeed, we will see below that the area Δ_2 must be rather closely specified in advance so that the chief freedom to be exercised by the designer is associated with Δ_1. The thought behind these observations is that whatever the approach, the design C_L and the distribution q(s)/U must be consistently prescribed.

We now turn to the properties of the flow in the neighborhoods of s_o and s_1 because at s_o the flow on the wetted surface is a stagnation flow and at s_1 it is constrained by the requirement for smooth separation. For simplicity's sake we shall shift our reference point from A_2 to the point 0 and measure the arc length s from 0. This means that the distance along the arc from 0 to A_1 is $s_1 - s_o$ and we will normalize all intermediate distances s by writing $x = s/(s_1 - s_o)$.

Then it is known for a potential-flow stagnation point on a flat wall that the streamlines are equilateral hyperbolas having their separatrices as the straight wall and the normal to the wall through the stagnation point. It is also known from linearized theory [9], and it can also be shown for the exact theory, that if $x = 1$ is a separation point then $C_p(x) \sim \sqrt{1 - x}$. A specific example of this general behavior can be seen by referring to the various formulae for the flat-plate velocity and pressure distributions given above in the discussion surrounding ω_o. In particular, it is easily seen that $dz/d\zeta = 0$ at the separation points $\zeta = \pm 1$. Consequently curves of q/U and C_p will have vertical tangents at the separation points. In response to these requirements we shall consider a one-parameter family of speed distributions on the forward part of the wetted surface; namely,

$$q(x)/U = x\left[1 - a\sqrt{1 - x^2}\left(1 - \sqrt{1 - x^2}\right)\right] \quad , \quad (0 \leq x \leq 1) \quad . \qquad (54)$$

Although this is a rather special class of velocity distributions, it probably contains as much generality as one usually needs because most often the arc length from s_o to s_1 is very small compared to the total arc length s_2. Therefore the curves of $q(x)/U$ will be very steep and the shape of one choice of distribution would hardly be discernible from some other choice, provided that the required conditions at $x = 0$ and $x = 1$ are satisfied. Plots of Eq. (54) are given for a highly stretched length scale in Fig. 11.

This specification and cavity surface velocity for $s_1 \leq s \leq s_2$ makes the entire pressure distribution on the upper surface of the profile fairly well defined. In order that these results can be used conveniently in the process of reconciling the design C_L with $q(s)/U$, Eq. (54) should be expressed in terms of the arc-length coordinates defined in Fig. 10. Normalizing all distances by s_2 we can write

$$x = \left(\frac{s_2}{s_1 - s_o}\right)\left(\frac{s - s_o}{s_2}\right) \quad . \tag{55}$$

Having prescribed the velocity distribution for points on the periphery of the profile, one can now use Eq. (20) in order to derive the circle-to-profile correlation between s_o and s_2 albeit with some degree of ambiguity until the entire problem has been formulated and solved. For this correlation, we will write Eq. (20) in the form,

$$\frac{q(s)}{U}\,ds = 2\,\frac{b^2}{U}\,(\cos\gamma - \cos\beta)\sin\beta\,d\beta = \frac{b^2}{U}\,d\left[(\cos\gamma - \cos\beta)^2\right] \quad , \tag{56}$$

where Eq. (54) defines $q(s)/U$ in the interval, $s_o \leq s \leq s_1$, and in the interval, $s_1 \leq s \leq s_2$, we have $q(s)/U = 1$. Moreover, at this point we know that when $s = s_o$, $\beta = \gamma$ and when $s = s_1$, $\beta = \pi$. From Eq. (55) we can put

$$(s_1 - s_o)dx = ds$$

and we can integrate Eq. (56) from $s_o (x = 0)$ to x and the right-hand side of Eq. (56) from $\beta = \gamma$ to β. Therefore the integral of Eq. (56) is

$$(s_1 - s_o)\left[\frac{x^2}{2} - a\left(\frac{1 - (1 - x^2)^{3/2}}{3} - \frac{x^2}{2} + \frac{x^4}{4}\right)\right] = \frac{b^2}{U}\,(\cos\gamma - \cos\beta)^2 \quad . \tag{57}$$

When $\beta = \pi$ and $x = 1$, Eq. (57) becomes

$$(s_1 - s_o)\left(1 - \frac{a}{6}\right) = 2\,\frac{b^2}{U}\,(1 + \cos\gamma)^2 \quad . \tag{58}$$

Proceeding to the arc $s_1 \leq s \leq s_2$ along the upper surface of the cavity one may start at the point $\beta = \pi$ on the circle $|\zeta| = 1$ and move along the negative real axis toward $\zeta = -r = 0$. The velocity $q/U = 1$ everywhere along this arc and Eqs. (19) can be used to find the differential arc-length correlation,

$$ds = -\frac{b^2}{U}\left[\frac{1}{2}\left(\frac{1}{r} + r\right) + \cos\gamma\right]\left(\frac{1}{r} - r\right)\frac{dr}{r} \quad , \tag{59}$$

where we have taken the positive square root in view of the fact that r has been defined as a positive quantity. Starting the integration at $s = s_1$ and $r = 1$, we find

$$s - s_1 = \frac{b^2}{U}\left\{\left(\frac{1}{r} - 1\right)\left[\frac{1}{4}\left(\frac{1}{r} + 1\right) + \cos\gamma\right] - (1 - r)\left[\frac{1}{4}(1 + r) + \cos\gamma\right]\right\} . \tag{60}$$

If $r = r_2$ when $s = s_2$ we can sum this special case of Eq. (60) and Eq. (58) in order to get expressions for Δ_2 in the profile and ζ planes. As implied from the outset, the considerations of this section apply to the inverse problem as a whole and we could extend the above considerations to deduce a correlation like (57) for the interval between A_2 and 0. We shall not complete the analysis here, however.

The Role of the Eigensolution

Returning to the eigensolution as given by Eq. (34a), we recall that except for the simple poles at $\zeta = e^{\pm i\gamma_c}$, the imaginary part of ω_c is zero everywhere on the unit circle and the real part suffers a jump of magnitude π at $\pm\gamma_c$ on the unit circle. On the other hand, we have found that the complex velocity has an isolated essential singularity at these poles (see

p. 22 above). Moreover, because of this fact we observed that q_c/U is bounded, being in the interval [0,1]. Therefore by appealing to a theorem of Weirestrass*, we shall assign the value $q_c/U = 1$ at the points $\gamma_c = \pm 1$ on $|\zeta| = 1$. We have also seen from an exploration of the flow due to an isolated eigensolution that the resulting profile is smooth and that its wetted surface is smooth. When the flat plate function ω_o and eigenfunction ω_c are combined, the resulting profile will also have a stagnation point at $\beta = \gamma$, as we shall discuss below.

As we have remarked above, our plan is to write the logarithmic hodograph as the sum of the flat plate function ω_o, the eigenfunction ω_c and a regular function ω_1. Thus

$$\omega(\zeta) = \omega_o + \omega_c + \omega_1 = \theta_o + \theta_c + \theta_1 + i\ell n \left[\frac{q_o}{U}\frac{q_c}{U}\frac{q_1}{U}\right] \quad . \tag{61}$$

Consequently,

$$\frac{q}{U} = \frac{q_o q_c q_1}{U^3} \quad . \tag{62}$$

The composite function, q/U, is prescribed from the outset. Equation (54) which has been defined over the arc length s in the interval $[s_o, s_1]$ corresponding to the normalized variable x in the interval [0,1], provides

---

*See for example, Copson, E. T., Theory of Functions of a Complex Variable Oxford University Press, 1946, p. 81; or Tichmarsh, The Theory of Functions, 2nd Edition, Oxford, 1949, pp. 93-94.

an example of such a composite function. The flat plate function, q_o/U, has been worked out on p. 17. Here it will be written as

$$\frac{q_o}{U} = \frac{2(-\cos\beta + \cos\gamma)}{(-\cos\beta + \cos\gamma)^2 + (\sin\beta + \sin\gamma)^2} \quad , \tag{63}$$

where the absolute sign in the numerator from p. 16 has been replaced by ordinary brackets and we have made other changes which apply in the interval $\gamma \leq \beta \leq \pi$. Since $q_c/U = 1$ on $|\zeta| = 1$ the function q_1/U follows from Eq. (62) rewritten as $q_1/U = (q/U)/(q_o/U)$. For the example at hand, the result of this transposition can not be used until we transform Eq. (63) from the ζ plane into the arc length in the interval $[s_o, s_1]$ with the help of Eq. (57). In particular, we find that

$$\sin^2\beta = 1 - (R - \cos\gamma)^2 = \sin^2\gamma + 2R\cos\gamma - R^2 \quad , \tag{64}$$

where

$$R^2 = \frac{U}{b^2}(s_1 - s_o)\left[\frac{x^2}{2} - a\left(\frac{1 - (1 - x^2)^{3/2}}{3} - \frac{x^2}{2} + \frac{x^4}{4}\right)\right] \quad .$$

Equation (64) enables us to write Eq. (63) in terms of arc length as

$$\frac{q_o}{U} = \frac{2R}{R^2 + \sin\gamma + \sqrt{\sin^2\gamma + 2R\cos\gamma - R^2}} \quad . \tag{65}$$

Then it follows from Eq. (62) that

$$\frac{q_1}{U} = \{(s_1 - s_o)x[1 - a\sqrt{1 - x^2}\,(1 - \sqrt{1 - x^2})]\} \div$$

$$\{2R/[R^2 + \sin\gamma + \sqrt{\sin^2\gamma + 2R\cos\zeta - R^2}]\} \quad . \qquad (66)$$

As is true of q_o/U and q_c/U, the function q_1/U when represented in the ζ plane can be continued to the arc of the unit circle in the lower half of the ζ-plane in accordance with the formulas at the bottom of p. 13.

Now that the well behaved function q_1/U has been found along the arc OA_1, we may return to Eq. (61) and note that the real part of $\omega(\zeta)$ is not yet known completely even in this interval. It will be known however, if we can find θ_1. But its complex conjugate τ_1 has just been found. Of course, we do not know τ_1 at all points of the unit circle because in this example we have have not prescribed the entire pressure distribution on the wetted surface, although the way in which this can be done is certainly clear. Once that step has been carried out, τ_1 will be known on the unit circle and its conjugate θ_1 can be calculated using the customary representation of $\omega_1(\zeta)$ as a Laurent expansion, as employed by Yoshihara [8] for example. Procedures which are preferable for practical engineering calculations are usually based on the Poisson integral formula or related methods. Examples of interest for the present inverse theory are given by Theodorsen and Garrick [16] and by Parkin and Peebles [17], among others. Further discussion of these matters is beyond the scope of this report.

In the course of designing a profile, the quantities which one specifies from the start are the design lift coefficient C_L, the pressure (velocity) distribution on the wetted surface, the cavity thickness at the trailing edge and perhaps the separation point of the upper surface of the cavity near the nose. The purpose of the eigensolution is to provide the necessary degrees of freedom which will permit the control of the cavity geometry as indicated. Added degrees of freedom can be incorporated in the prescribed pressure distribution if a parametric approach is used. It might be possible to lower the cavity drag somewhat by adjusting them although the prescription of cavity thickness is probably more important in this regard. The outcome of the design process will be coordinates of the profile and cavity shape, including the separation point; the attack angle, α; and the drag coefficient C_D. The eigensolution strength, E/b, will also be determined in the course of the calculations.

Conclusions

The chief finding of this paper is that one can construct many singular eigensolutions for the exact inverse problem of two-dimensional cavity flow at zero cavitation number. From among these, we have chosen that single eigensolution which provides the correct branching of the flow at its singularity, it also appears to offer the least disturbance to the upstream flow field inclination of any cavity flow which does not already include a point-drag solution as one of its elements. This particular choice also seems to offer the greatest analytical convenience. The physical conditions satisfied by this eigensolution are:

(1) At points on the cavity and on the wetted surface of the profile, the flow velocity is equal in magnitude to the free-stream velocity. Consequently, except for the singular point the pressure coefficient is zero on the wetted and cavity surfaces.

(2) The point-drag solution vanishes at infinity, but it does have a bounded essential singularity on the wetted surface and it produces no singular velocities or pressures in the flow.

(3) This function produces no additional flow inclination on the entire upstream stagnation streamline.

A specific example of the flow geometry represented by an isolated eigensolution has been given above to show how this function can produce round-nosed profiles. In general, it is found that the point-drag solution produces a widening of the cavity which is directly proportional to its strength. An incremental cavity drag accompanies this widening and this drag is proportional to the square of the eigensolution strength. No lift is produced by the point-drag function when its location coincides with that of the stagnation point on the profile surface. In contrast to the linearized theory, the complementary function singularity need not be at the stagnation point. In these cases, the incremental cavity drag is not changed from its value when the singularity is at the stagnation point. But when the singularity is located between the stagnation point and the upper separation point a negative incremental lift is produced. If the singularity is on the lower surface, downstream of the stagnation point,

a positive lift increment is found. Whether or not it is better to position the eigensolution at some point on the profile instead of at the stagnation point remains to be studied.

As a result of these findings, it appears that an eigensolution exists for the nonlinear theory of cavity flow at zero cavitation number and that it is now most likely that a similar eigensolution can be found for such fully cavitating flows at cavitation numbers which are greater than zero. The results found so far suggest that the nonlinearized theory and the linearized theories parallel one another very closely as far as the nature of their point drag solutions are concerned. But the present results exhibit some featues which are lost in the process of linearization.

References

1. Yim, B and L. Higgins, "A Nonlinear Design Theory of Supercavitating Cascades," Transactions of the ASME, Journal of Fluids Engineering, Vol. 97, Series I, No. 4, p. 430 (December 1975).

2. Khrabov, I. A., "Plane Problems of Cavitation Flow Around an Oblique Cascade of Profiles," Izvestiya Akademii Nauk SSSR, Mekhanika Zhidkosti i Gaza, No. 3, pp. 149-152 (May-June 1975). Translated: Plenum Publishing Corporation, 227 West 17th Street, New York (1977).

3. Furuya, O., "Exact Supercavitating Cascade Theory," Transactions of the ASME, Journal of Fluids Engineering, Vol. 97, Series I, No. 4, p. 430 (December 1975).

4. Durand, W. F. (Ed.), Aerodynamic Theory, Vol. II, by Th. Von Karman and J. M. Burgers, Dover Publications, Inc., New York, pp. 336-339 (1963).

5. Gurevich, M. I., Theory of Jets in Ideal Fluids, Academic Press, New York, pp. 131-143 (1965).

6. Woods, L. C., The Theory of Subsonic Plane Flow, Cambridge University Press, London, pp. 443-454 (1961).

7. Milne-Thomson, L. M., Theoretical Hydrodynamics, Fifth Edition, The MacMillan Press, Ltd., London, pp. 338-348 (1968).

8. Yoshihara, H., "Optimum Fully Cavitated Hydrofoils at Zero Cavitation Number," Journal of Aircraft, Vol. 3, No. 4, p. 372 (1966).

9. Parkin, B. R. and R. S. Grote, "Inverse Methods in the Linearized Theory of Fully Caviting Hydrofoils," Transactions of the ASME, Journal of Basic Engineering, Vol. 86, Series D, No. 4 (December 1964).

10. Parkin, B. R. and J. Fernandez, "A Third Procedure for Linearized Fully-Cavitating Hydrofoil Section Design," ARL Technical Memorandum, File No. TM 77-186, Applied Research Laboratory, The Pennsylvania State University (5 July 1977).

11. Parkin, B. R., "An Extended Linearized Inverse Theory for Fully Cavitating Hydrofoil Section Design," J. Ship Research, p. 260 (December 1979).

_____, "Hydrodynamic Trends from a Generalized Design Procedure for Fully Cavitating Hydrofoil Sections," J. Ship Research, p. 272 (December 1979).

12. Lamb, Sir Horace, Hydrodynamics, Sixth Edition, Dover Publications, New York, pp. 102-103 (1945).

13. Parkin, B. R., "Munk Integrals for Fully Cavitated Hydrofoils," J. of the Aerospace Sciences, Vol. 29, No. 7, p. 775 (July 1962).

14. Tulin, Marshall P., "Supercavitating Flows -- Small Perturbation Theory," J. Ship Research, p. 272 (January 1964).

15. Fabula, A. G., "Fundamental Step Profiles in Thin-Airfoil Theory with Hydrofoil Application," J. Aerospace Sciences, Vol. 28, No. 6 (June 1961).

16. Theodorsen, T. and I. E. Garrick, "General Potential Theory of Arbitrary Wing Sections," NACA Technical Report No. 452.

17. Parkin, B. R. and G. H. Peebles, "Calculation of Hydrofoil Sections for Prescribed Pressure Distributions," Technical and Research Bulletin No. 1-17, The Society of Naval Architects and Marine Engineers (1956).

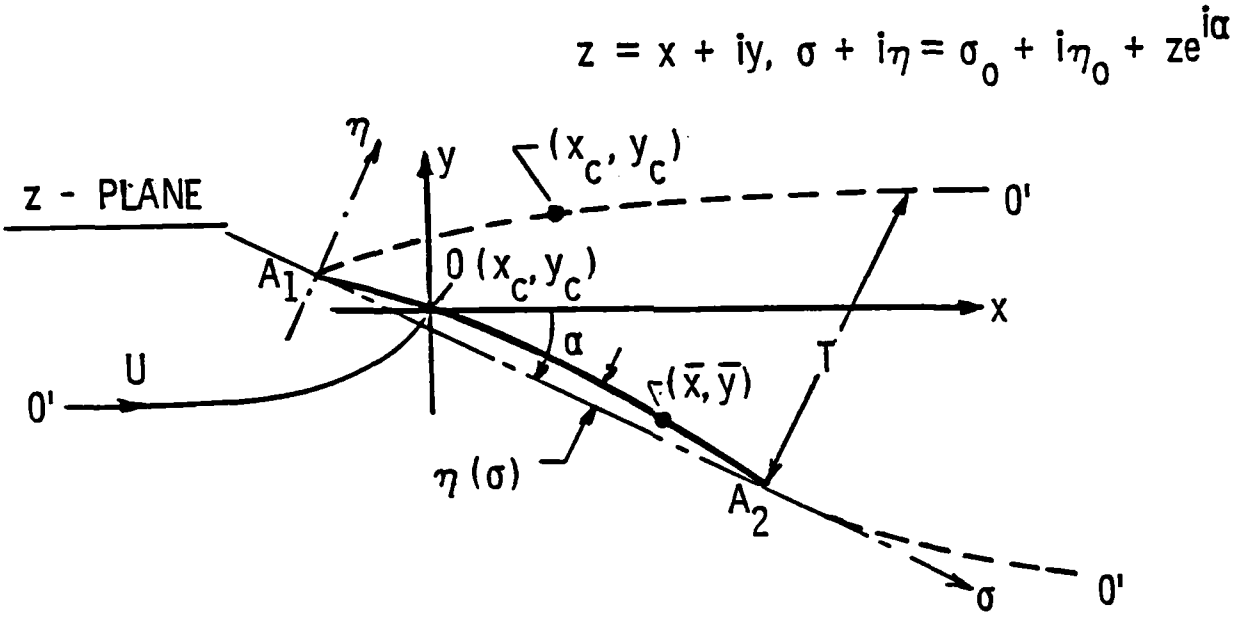

Figure 1. Profile and cavity geometry in the physical or z-plane at zero cavitation number.

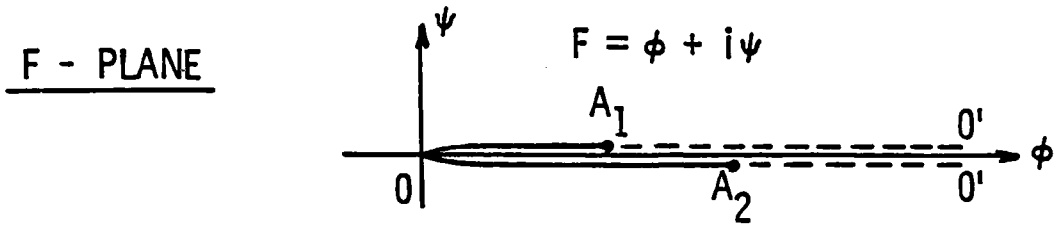

Figure 2. Profile and cavity surfaces at zero cavitation number in the plane of the complex potential, $F = \phi + i\psi$.

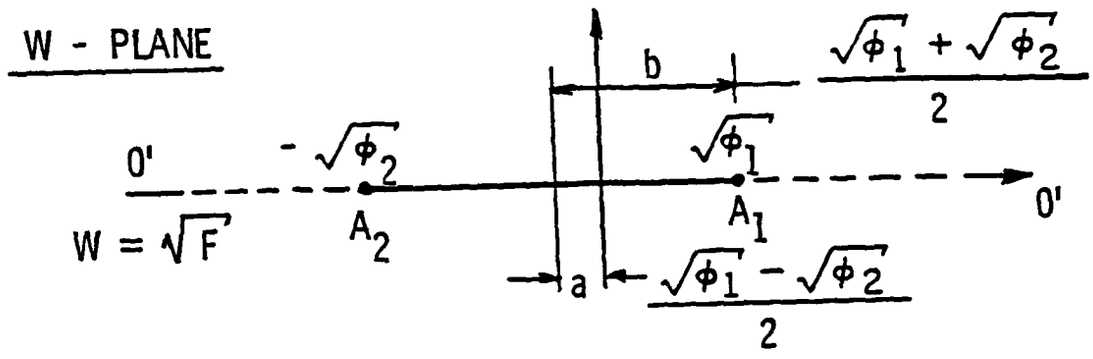

Figure 3. The mapping $W = \sqrt{F}$ maps the flow outside the cut in the F plane into the upper half W plane.

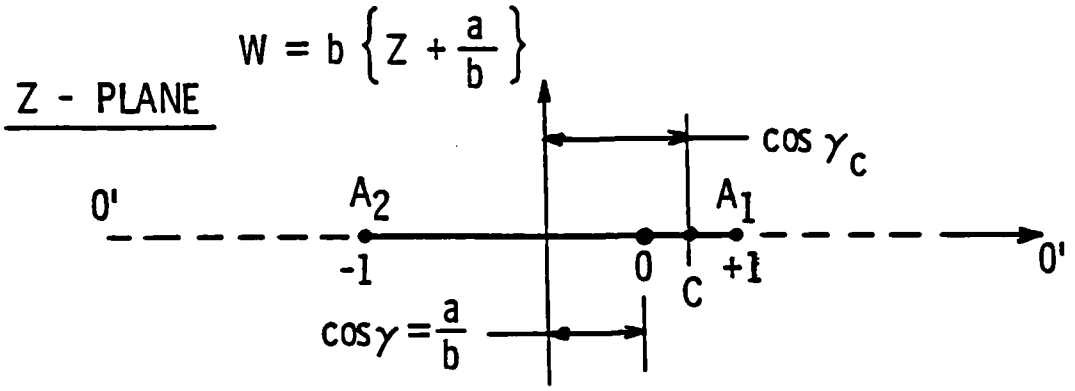

Figure 4. The wetted surface lies between -1 and +1 in the complex Z plane.

$$Z = -\frac{1}{2}\left(\zeta + \frac{1}{\zeta}\right) \qquad \zeta = -Z + \sqrt{Z^2-1}$$

$$F = b^2\left[\frac{1}{2}\left(\zeta + \frac{1}{\zeta}\right) - \cos\gamma\right]^2$$

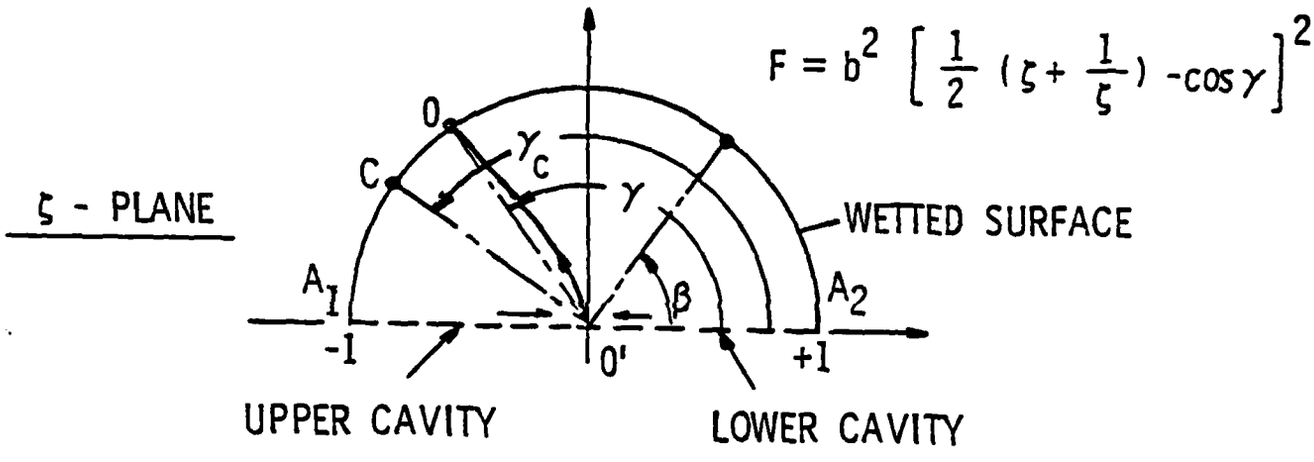

Figure 5. The Joukowski transformation maps the flow from the upper half of the Z-plane into the interior of the upper unit semi-circle with the point at infinity at the origin.

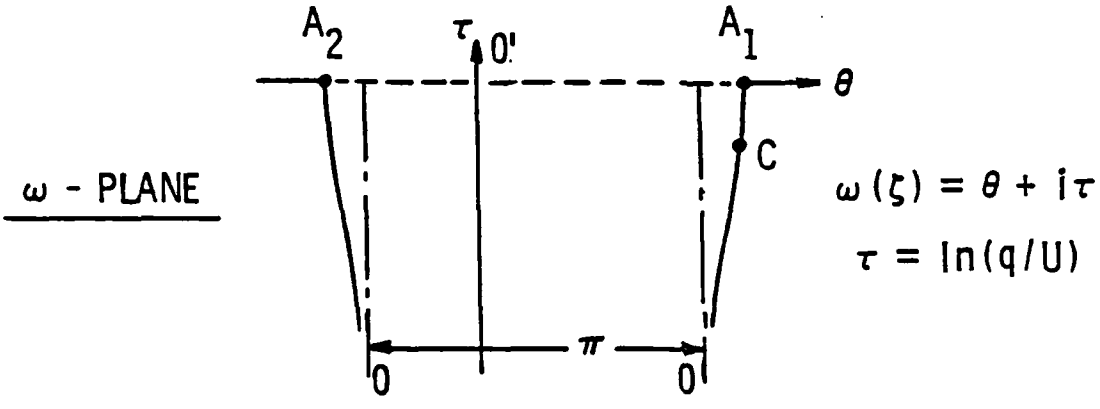

Figure 6. Schematic diagram of the complex logarithmic hodograph in the ω-plane.

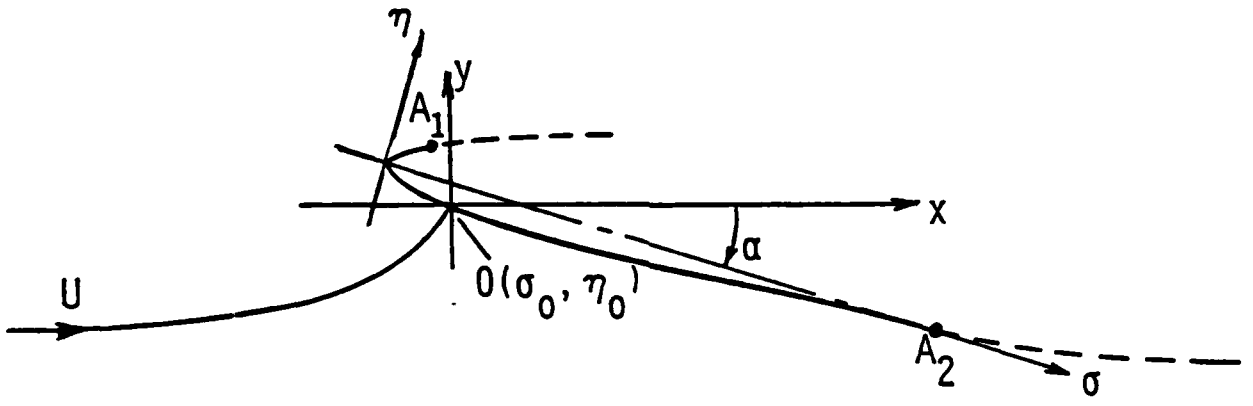

Figure 7. The geometry of a round-nosed profile of unit chord showing the origin of $\sigma - \eta$ coordinates at the apex of the wetted surface corresponding to (x_a, y_a) in z-plane coordinates.

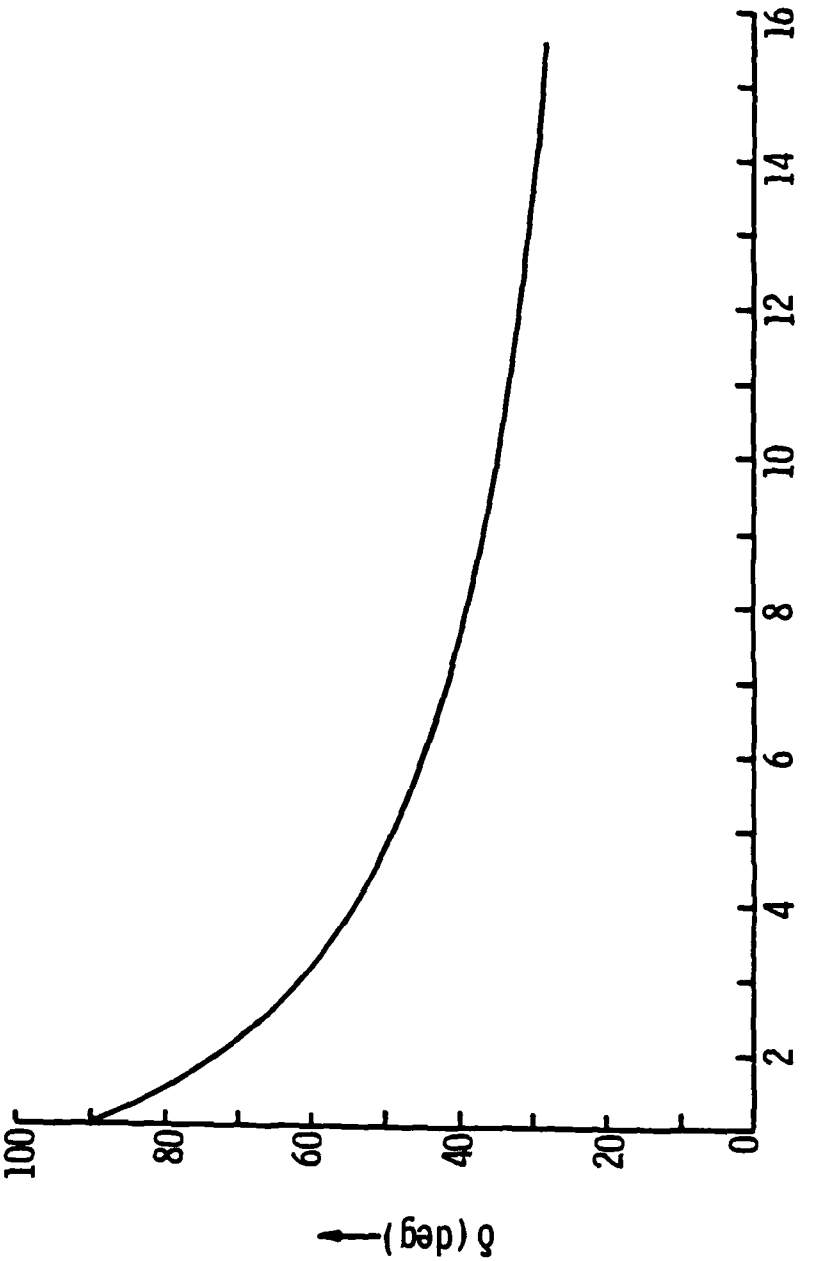

Figure 8. Angular location, δ, of the stagnation point vs the parameter n for the isolated eigensolution.

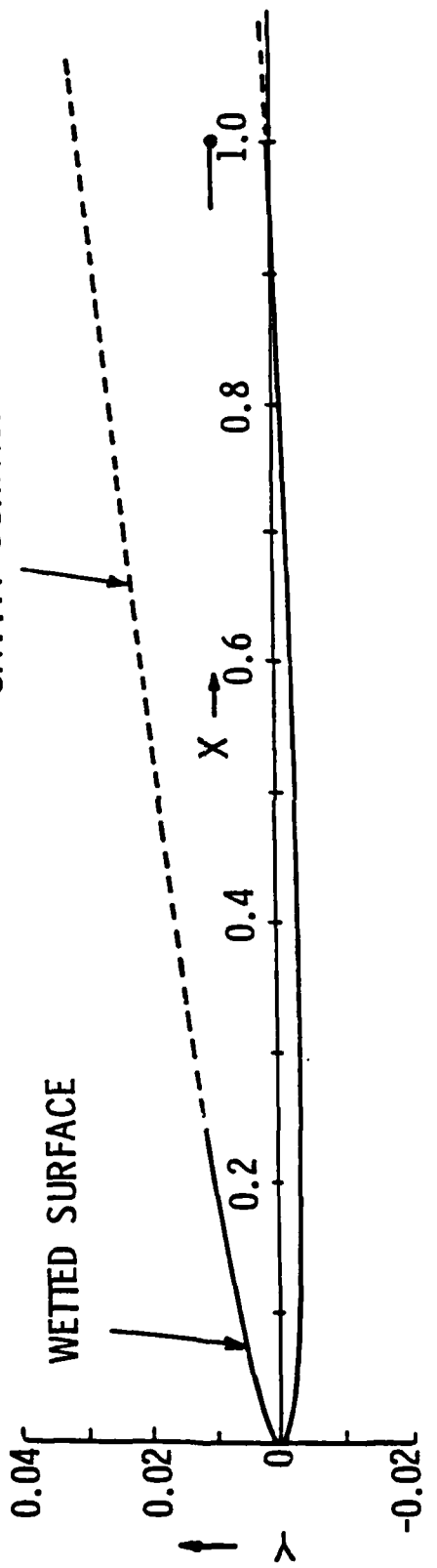

Figure 9. The profile and cavity contours produced by an isolated eigensolution of strength $\frac{E}{b} = .01$ at the stagnation point $\delta = 70°$ which produces a cavity drag $C_{D_c} = .0035$ and cavity thickness $T = .0298$. Note the distortion of the vertical scale in the plot. The line and dot at X = 1 show the true geometry when the vertical and horizontal axes have the same scale.

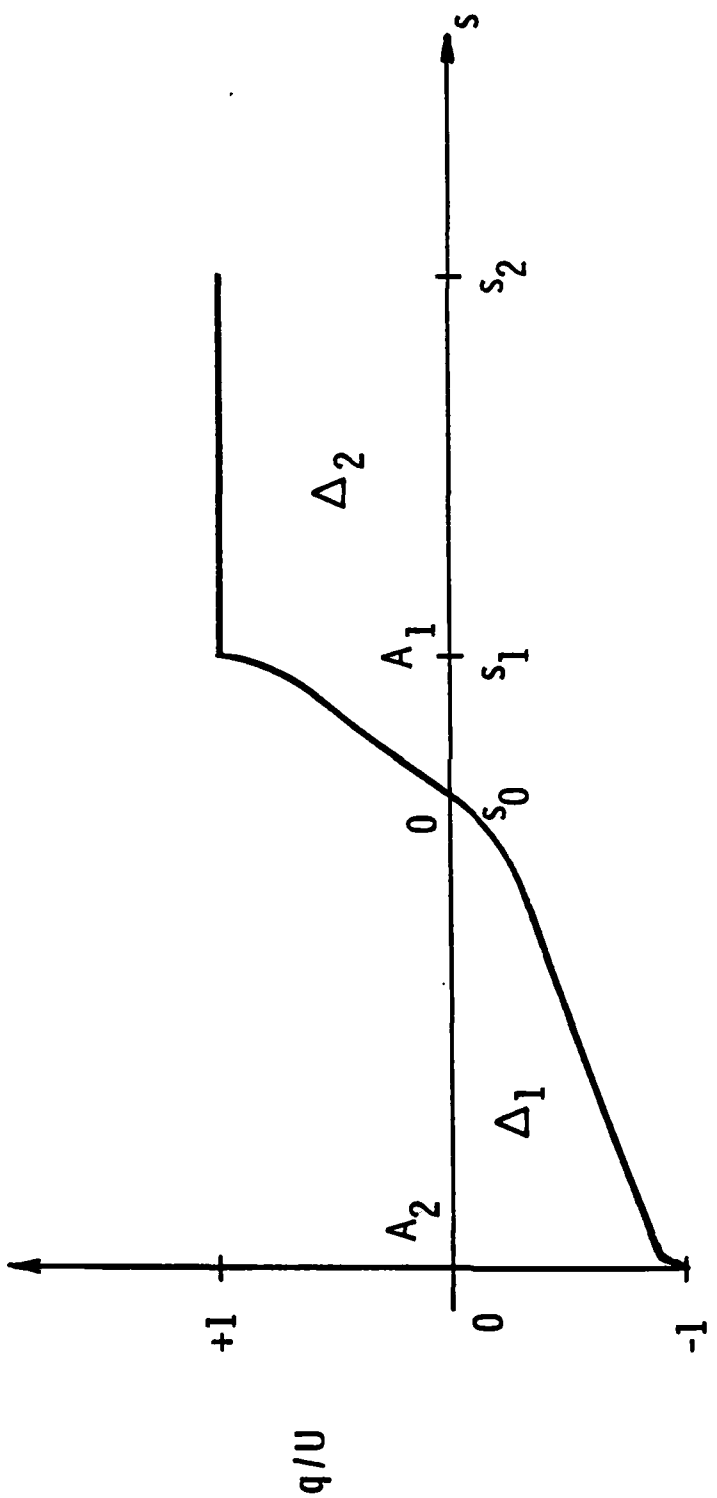

Figure 10. Schematic diagram showing a prescribed velocity distribution on a profile and cavity arc.

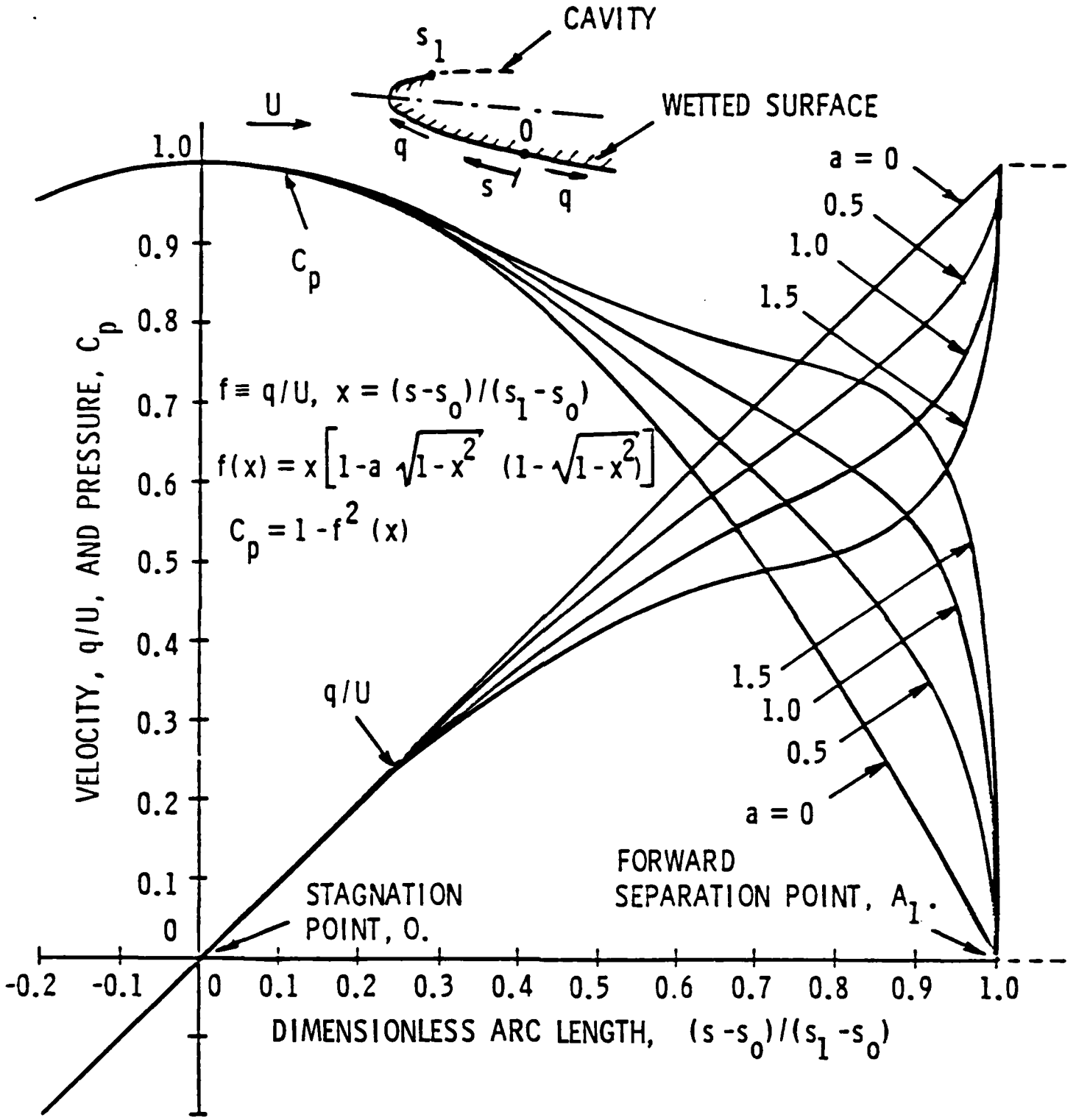

Figure 11. A one-parameter family of velocity and pressure distributions over the nose arc of a hydrofoil.

DISTRIBUTION LIST FOR UNCLASSIFIED TECHNICAL MEMORANDUM 85-97,
by B. R. Parkin, dated 5 June 1985

Defense Technical Information
Center
5010 Duke Street
Cameron Station
Alexandria, VA 22314
(Copies 1 through 6)

Commanding Officer
David W. Taylor Naval Ship
Research & Development Ctr.
Department of the Navy
Bethesda, MD 20084
Attention: M. Tod Hinkel
Code 1504
(Copies 7 through 12)

Commander
Naval Sea Systems Command
Department of the Navy
Washington, DC 20362
Attention: T. E. Peirce
Code NSEA-63R31
(Copy No. 13)

Director
Applied Research Laboratory
The Pennsylvania State University
Post Office Box 30
State College, PA 16804
Attention: M. L. Billet
(Copy No. 14)

Director
Applied Research Laboratory
The Pennsylvania State University
Post Office Box 30
State College, PA 16804
Attention: L. R. Hettche
(Copy No. 15)

Director
Applied Research Laboratory
The Pennsylvania State University
Post Office Box 30
State College, PA 16804
Attention: J. W. Holl
(Copy No. 16)

Director
Applied Research Laboratory
The Pennsylvania State University
Post Office Box 30
State College, PA 16804
Attention: B. R. Parkin
(Copy No. 17)

Director
Applied Research Laboratory
The Pennsylvania State University
Post Office Box 30
State College, PA 16804
Attention: GTWT Files
(Copy No. 18)

Director
Applied Research Laboratory
The Pennsylvania State University
Post Office Box 30
State College, PA 16804
Attention: ARL/PSU Library
(Copy No. 19)

END

FILMED

12-85

DTIC